

②

NAVAL POSTGRADUATE SCHOOL

Monterey, California

AD-A202 006

DTIC FILE COPY



THESIS

Two-Dimensional Computation of Heat Transfer
in Fusion Welding

by

Lambert Roger Walker III

September 1988

Thesis Advisor:

Yogendra Joshi

Approved for public release; distribution is unlimited

DTIC
ELECTE
S 0 4 JAN 1989 D
C
E

89 1 04 024

Unclassified

Security Classification of this page

REPORT DOCUMENTATION PAGE

1a Report Security Classification Unclassified		1b Restrictive Markings	
2a Security Classification Authority		3 Distribution Availability of Report Approved for public release; distribution is unlimited.	
2b Declassification/Downgrading Schedule		5 Monitoring Organization Report Number(s)	
4 Performing Organization Report Number(s)		7a Name of Monitoring Organization Naval Postgraduate School	
6a Name of Performing Organization Naval Postgraduate School	6b Office Symbol (If Applicable) 69	7b Address (city, state, and ZIP code) Monterey, CA 93943-5000	
6c Address (city, state, and ZIP code) Monterey, CA 93943-5000		9 Procurement Instrument Identification Number	
8a Name of Funding/Sponsoring Organization	8b Office Symbol (If Applicable)	10 Source of Funding Numbers	
8c Address (city, state, and ZIP code)		Program Element Number	Project No Task No Work Unit Accession No
11 Title (Include Security Classification) Two-Dimensional Computation of Heat Transfer in Fusion Welding			
12 Personal Author(s) Lambert Roger Walker III			
13a Type of Report Master's Thesis	13b Time Covered From To	14 Date of Report (year, month, day) September 1988	15 Page Count 112
16 Supplementary Notation The views expressed in this thesis are those of the author and do not reflect the official policy or position of the Department of Defense or the U.S. Government.			
17 Cosati Codes		18 Subject Terms (continue on reverse if necessary and identify by block number)	
Field	Group	Subgroup	
		Fusion Welding, Heat Transfer, Finite Difference Analysis, Using Enthalpy Formulation	
19 Abstract (continue on reverse if necessary and identify by block number) A two-dimensional finite difference model was developed to calculate the temperature distribution during the fusion welding process. The model is based upon the enthalpy formulation for phase change processes. Changes in thermal properties during the process have been accounted for. Temperature variations with respect to time have been calculated for specific locations in the cross-section of the work piece away from the edges for specified boundary conditions. These computations allow the estimation of cooling rates and the extent of the fusion zone. The model could be used in real-time monitoring of the welding process. <i>Thesis</i>			
20 Distribution/Availability of Abstract <input checked="" type="checkbox"/> unclassified/unlimited <input type="checkbox"/> same as report <input type="checkbox"/> DTIC users		21 Abstract Security Classification Unclassified	
22a Name of Responsible Individual Y. Joshi		22b Telephone (Include Area code) (408) 646-3400	22c Office Symbol 69Ji

DD FORM 1473, 84 MAR

83 APR edition may be used until exhausted

security classification of this page

All other editions are obsolete

Unclassified

Approved for public release; distribution is unlimited.

Two-Dimensional Computation of Heat Transfer in Fusion Welding

by

Lambert Roger Walker III
Lieutenant Commander, United States Navy
B.S.Mar.E., United States Naval Academy, 1975

Submitted in partial fulfillment of the
requirements for the degree of

MASTER OF SCIENCE IN MECHANICAL ENGINEERING

from the

NAVAL POSTGRADUATE SCHOOL
September 1988

Author:

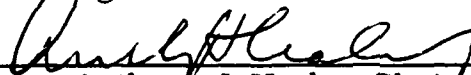


Lambert Roger Walker III

Approved by:



Yogendra Joshi, Thesis Advisor



Anthony J. Healey, Chairman,
Department of Mechanical Engineering



Gordon E. Schacher, Dean of
Science and Engineering

ABSTRACT

A two-dimensional finite difference model was developed to calculate the temperature distribution during the fusion welding process. The model is based upon the enthalpy formulation for phase change processes. Changes in thermal properties during the process have been accounted for. Temperature variations with respect to time have been calculated for specific locations in the cross-section of the work piece away from the edges for specified boundary conditions. These computations allow the estimation of cooling rates and the extent of the fusion zone. The model could be used in real-time monitoring of the welding process.

Accession For	
NTIS GRA&I	<input checked="" type="checkbox"/>
DTIC TAB	<input type="checkbox"/>
Unannounced	<input type="checkbox"/>
Justification	
By	
Distribution/	
Availability Codes	
Dist	Avail and/or Special
A-1	



TABLE OF CONTENTS

I. INTRODUCTION.....	1
A BACKGROUND.....	1
B PREVIOUS STUDIES.....	2
C MODELING THE HEAT FLOW.....	4
II. TWO-DIMENSIONAL FINITE DIFFERENCE MODEL.....	5
A OBJECTIVES.....	5
B ENTHALPY FORMULATION.....	7
1. Derivation of Nodal Finite Difference Equations	7
C SPECIAL CONSIDERATIONS.....	13
1. Non-Uniform Grid Spacing.....	13
2. Modeling the Welding Torch Arc.....	13
D SOLUTION PROCEDURE	17
III. RESULTS.....	20
A PARAMETERS.....	20
B DISCUSSION.....	21
IV. CONCLUSIONS.....	24
APPENDIX A MODEL EQUATIONS.....	25
APPENDIX B MATERIAL DATA.....	30

APPENDIX C	COMPUTER PROGRAM OF MODEL.....	33
APPENDIX D	DATA	46
LIST OF REFERENCES	103
INITIAL DISTRIBUTION LIST	105

LIST OF FIGURES

1	Work Piece Schematic.....	6
2	Control Volume Diagram for Interior Points.....	10
3	Control Volume Diagram for Top Wall Points Exposed to External Heat Flux.....	11
4	Control Volume Diagram for NW Corner Point	12
5	Non-Uniform Grid Illustration.....	14
6	Welding Torch Arc	15
7	Comparison of Computational Results and Data from Kihara for Center-Line Surface Temperatures After the Heat Source Has Completely Passed the Center-Line Surface Node.....	23

I. INTRODUCTION

A. BACKGROUND

The welding process in most applications is largely dependent upon the skill of the welder with regard to the quality and accuracy of the weld. Control of the voltage and current settings and the speed at which the torch advances can significantly affect the welding process. An experienced welder can adjust these parameters based upon the conditions he observes during the process. As the experience level varies from welder to welder, the quality of the weld can vary also. An unsatisfactory weld will result in expensive and time-consuming rework, assuming that the flaw is detected and identified. If the flaw remains undetected, catastrophic failure may occur at some future time. Neither of these situations is desirable. If a reliable automated system can be developed that produces uniform and repeatable results for a specified set of conditions, the reliability of the welding process will increase and the long-term costs will decline.

To support automating the process, a simple means of monitoring the weld is desired. One way of sensing what is occurring in the weld process is to monitor the heat flow patterns on the material being welded. If the heat flow patterns for a high-quality weld are established, the amount of deviation of the actual weld heat flow patterns from the established values can be used as a measure of the quality of the weld. When the quality level reaches a level considered

unsatisfactory, a control system can be used to provide real-time corrective action. This area has been the subject of several studies.

B. PREVIOUS STUDIES

The first significant studies of heat flow in welding were conducted by Rosenthal starting in the late 1930s. Rosenthal investigated both point and line heat sources as idealizations of the welding process. Results of such analyses are only applicable far away from the heat sources. Between 1940 and 1980, there were several studies of heat transfer during the welding process, as described by Koichi Masubuchi [Ref. 1].

W. H. Giedt explored the problem of modeling a control system for the Gas-Tungsten-Arc welding process [Ref. 2]. A two-dimensional model originally proposed in Reference 3 is assumed to be a reasonable approximation of the heat flow in a work piece being welded. The two-dimensional model was chosen over the more-exact three-dimensional model, primarily due to the reduced computational time that is required. For such a system to be practical, the welding system should be portable. A portable computer implies reduced computational speed from a large mainframe computer, thus the emphasis on reduced computational time.

Goldak, Chakravarti, and Bibby have taken the welding model a step further by modifying the grid pattern used [Ref. 4]. In order to improve the ability of the model to accommodate both shallow and deep penetration welds, the authors developed a non-axisymmetric, three-dimensional, heat-source model. To accommodate the new heat

source, the grid pattern changed from rectangular to ellipsoid. This approach resulted in values that were closer to experimental values for both deep and shallow penetration welds than previous models. However, the model became significantly more complicated to achieve the increased accuracy.

Kou and Le present a three-dimensional heat flow model for a pipe undergoing a seam weld [Ref. 5]. This model addressed the problem of weld pool convection by using an "effective" thermal conductivity to account for the effect of convection within the weld pool on the heat flow.

Oreper and Szekely delve more fully into the circulation patterns that occur within a weld pool [Ref. 6]. Their analysis centers around three key components. The heat flow must be modeled in both solid and molten regions. In the molten regions, fluid flow must take into account buoyancy, surface tension, and electromagnetic forces.

The predictions from a computational model must be experimentally verified. Masubuchi [Ref. 1] describes several studies on temperature measurement using thermocouples. Khan, et al., discuss the use of an infrared sensor to monitor weld surface temperatures [Ref. 7]. Infrared imaging of the surface area around the point of application of the weld torch provided a means of monitoring temperatures throughout this small area. As pointed out by them, the resolution of such a system must be sufficient to discriminate between disturbances that would affect weld quality and system noise. Additionally, the time constant of the system must be sufficiently small to be able to react to

a detected problem before the torch has passed the region of the flaw. Unless the problem is corrected while the area is still molten, it will not be correctable. The need for a realistic model of the welding process for real-time control is clear from the study by Khan, et al. [Ref. 7].

C. MODELING THE HEAT FLOW

In order for a real-time control system to be effective, the model must provide accurate data about the heat flow in the work piece. The model developed in the present study calculates enthalpy and temperature values in a vertical cross-sectional plane of the work piece. The data is delivered as temperature at each nodal location. Surface temperature data are obtained from a time history of such cross-sections.

The flow of heat within the work piece includes several complex interactions. In the solid phase, conduction, surface convection, and radiation constitute the heat transfer nodes. In the molten region, liquid phase material is subject to added effects caused by weld pool circulation [Ref. 6]. The need for simplifying assumptions becomes evident when computational speed is necessary, as in real-time control applications. These are discussed in the following chapter.

II. TWO-DIMENSIONAL FINITE DIFFERENCE MODEL

A. OBJECTIVES

The present study examines a two-dimensional model which simulates the heat flow in a cross-section of a work piece during the autogenous (no filler metal) welding of a butt joint with no contact resistance (see Figure 1). The model starts with all temperatures in the cross-section at ambient conditions. As the leading edge of the welding torch reaches the plane of the cross-section, energy is added to the cross-section from the top surface, initially at an increasing rate. As the center of the torch passes the cross-section, the energy added decreases until none is being added when the trailing edge of the torch has passed the cross-section. The entire surface area of the slab is considered to have free convection with the ambient environment. Additionally, the entire surface area is able to radiate to the environment.

The model takes into consideration the effects of phase changes within the work piece. This is accomplished by using an enthalpy formulation. The model also accommodates various geometric dimensions, welding parameters (current, voltage, efficiency, torch speed of advance, etc.), and material properties. The accuracy to which the location of the reported temperature is determined could be varied by changing the number of nodes at which temperature is calculated.

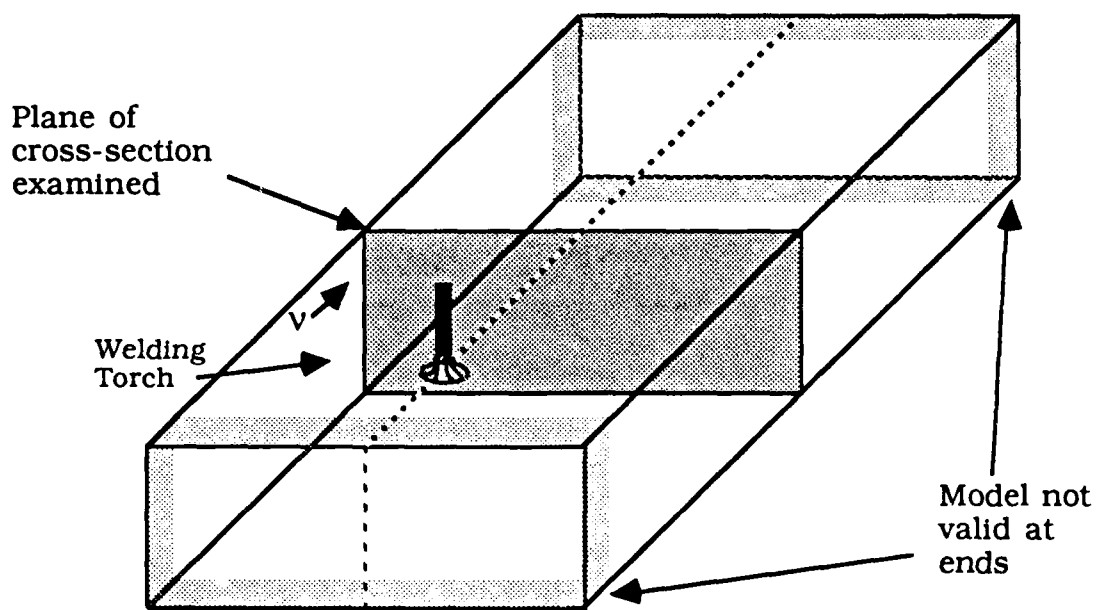


Figure 1. **Work Piece Schematic**

A two-dimensional finite difference model was chosen in this study due to its simplicity and faster computational speed.

B. ENTHALPY FORMULATION

Welding, by its very nature, involves a phase change from solid to liquid and eventually back to solid. Models considering uniform specific heat have no way of accounting for the latent heat of fusion absorbed by the material as it melts once it has reached melting temperature. The temperature of the molten material will not rise above the melting temperature until its enthalpy has reached the sum of the melting enthalpy and the latent heat of fusion. By using the enthalpy at each node instead of the temperature in the storage term of the energy equation, phase changes can be easily accommodated and the temperature can be determined at each time step. This technique has been employed in the current computation. It is described in detail in Reference 9.

1. Derivation of Nodal Finite Difference Equations

There are several categories of nodal finite difference equations for the model of a rectangular slab. These include interior nodes, surface nodes not subject to a heat flux, surface nodes subjected to a heat flux, and surface corner nodes. The equations for the interior nodes, a surface node with heat flux, and a surface corner node are developed in detail next. The equations for all the categories can be found in Appendix A.

All of the categories start with an appropriate energy balance over the control volume being considered. For an interior control volume, this leads to:

$$\frac{\partial}{\partial x} \left(k \frac{\partial T}{\partial x} \right) + \frac{\partial}{\partial y} \left(k \frac{\partial T}{\partial y} \right) = \frac{\partial H}{\partial t} \quad (1)$$

Since the thermal conductivity is a function of temperature, it will vary with location as the temperature at that location changes. This change in thermal conductivity with location is handled by calculating an interface conductivity for a position halfway between the node being investigated and each of its adjacent neighbors. This value is referred to as the harmonic mean value [Ref. 9]. For example, the conductivity between node (i,j) and node (i-1,j) is found as follows:

$$\begin{aligned} q_{i-\frac{1}{2},j} &= - \left(k \frac{\partial T}{\partial x} \right)_{i-\frac{1}{2},j} = \frac{k_{i-\frac{1}{2},j} (T_{i-1,j} - T_{i,j})}{\frac{1}{2}(\Delta XL + \Delta X)} \\ &= \frac{(T_{i-1,j} - T_{i,j})}{\frac{\Delta XL}{2k_{i-1,j}} + \frac{\Delta X}{2k_{i,j}}} = \frac{(T_{i-1,j} - T_{i,j})}{\frac{k_{i,j}\Delta XL + k_{i-1,j}\Delta X}{2k_{i-1,j}k_{i,j}}} \end{aligned} \quad (2)$$

Therefore:

$$\frac{k_{i-\frac{1}{2},j}}{\frac{1}{2}(\Delta XL + \Delta X)} = \frac{k_{i-1,j}k_{i,j}}{\frac{1}{2}(k_{i,j}\Delta XL + k_{i-1,j}\Delta X)} \quad (3)$$

or

$$K1 = k_{i-\frac{1}{2},j} = \frac{k_{i-1,j}k_{i,j}(\Delta XL + \Delta X)}{k_{i,j}\Delta XL + k_{i-1,j}\Delta X} \quad (4)$$

where ΔX is distance in X direction across node (i,j), and

ΔX_L is the distance in X direction from center of node (i,j) to center of node (i-1,j).

A similar procedure is followed for each value of conductivity appropriate to each of the four boundaries of the nodal square (see Figure 2). The equations for each conductivity can be found in Appendix A. The energy balance equation for an interior node becomes:

$$\begin{aligned} & \frac{K1 * (T(I-1,J) - T(I,J)) * \Delta Y}{\Delta X_L} + \frac{K2 * (T(I,J-1) - T(I,J)) * \Delta X}{\Delta Y_T} \\ & + \frac{K3 * (T(I+1,J) - T(I,J)) * \Delta Y}{\Delta X_R} + \frac{K4 * (T(I,J+1) - T(I,J)) * \Delta X}{\Delta Y_B} \quad (5) \\ & = \frac{H^{n+1}(I,J) - H^n(I,J)}{\Delta t} \end{aligned}$$

$$\begin{aligned} H^{n+1}(I,J) = & \Delta t * (K1 * T(I-1) * \Delta Y / \Delta X_L + K2 * T(I,J-1) * \Delta X / \Delta Y_T \\ & + K3 * T(I+1,J) * \Delta Y / \Delta X_R + K4 * T(I,J+1) * \Delta X / \Delta Y_B \\ & - (K1 * \Delta Y / \Delta X_L + K2 * \Delta X / \Delta Y_T + K3 * \Delta Y / \Delta X_R \\ & + K4 * \Delta X / \Delta Y_B) * T(I,J)) + H^n(I,J) \quad (6) \end{aligned}$$

The energy balance for a top wall node exposed to flux Q becomes (see Figure 3):

$$\begin{aligned} & \frac{K1 * (T(I-1,J) - T(I,J)) * \frac{\Delta Y}{2}}{\Delta X_L} + Q * \Delta X + \frac{K3 * (T(I+1,J) - T(I,J)) * \frac{\Delta Y}{2}}{\Delta X_R} \\ & + \frac{K4 * (T(I,J+1) - T(I,J)) * \Delta X}{\Delta Y_B} = \frac{H^{n+1}(I,J) - H^n(I,J)}{\Delta t} \quad (7) \end{aligned}$$

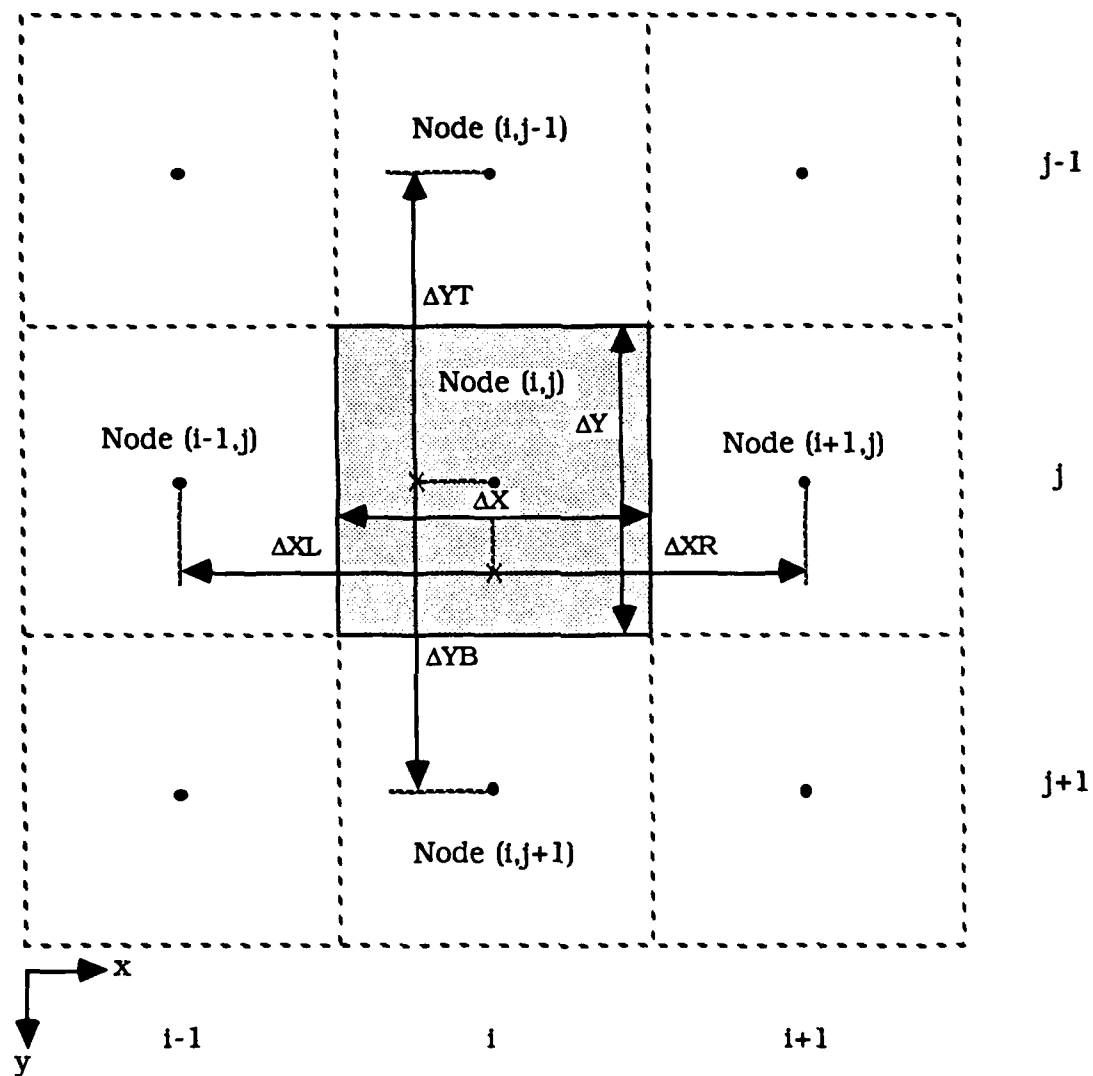


Figure 2. Control Volume Diagram for Interior Points

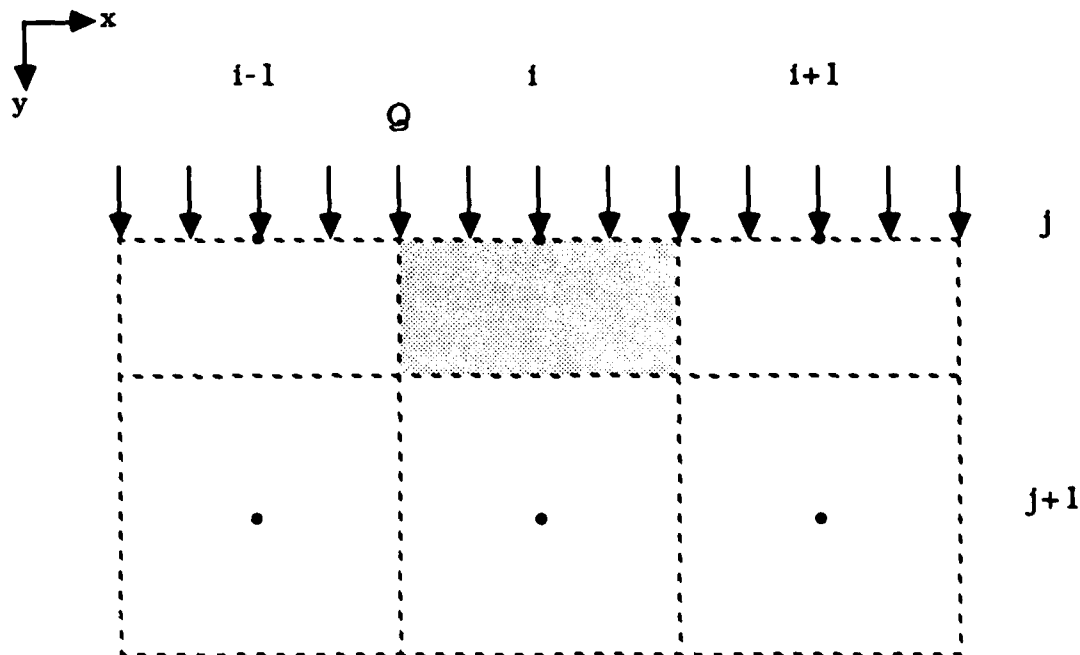


Figure 3. Control Volume Diagram for Top Wall Points Exposed to External Heat Flux

$$\begin{aligned}
 H^{n+1}(I,J) = & \Delta t * (Q * \Delta X + K1 * T(I - 1,J) * \Delta Y / (2 * \Delta XL) \\
 & + K3 * T(I + 1,J) * \Delta Y / (2 * \Delta XR) + K4 * T(I,J + 1) \\
 & * \Delta X / \Delta YB - (K1 * \Delta Y / (2 * \Delta XL) + K3 * \Delta Y / (2 * \Delta XR) \\
 & + K4 * \Delta X / \Delta YB) * T(I,J)) + H^n(I,J)
 \end{aligned} \tag{8}$$

The energy balance for a surface corner node becomes (see Figure 4):

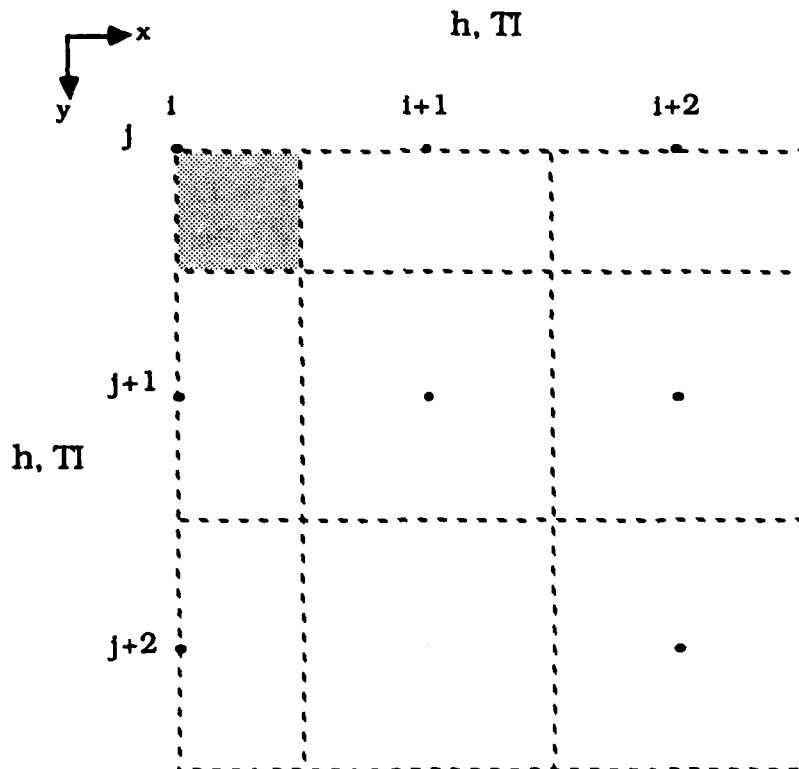


Figure 4. Control Volume Diagram for NW Corner Point

$$\begin{aligned}
 & h * (T_I - T(I, J)) * \frac{\Delta X}{2} + h * (T_I - T(I, J)) * \frac{\Delta Y}{2} \\
 & + \frac{K_3 * (T(I+1, J) - T(I, J))}{\Delta X_R} * \frac{\Delta Y}{2} \\
 & + \frac{K_4 * (T(I, J+1) - T(I, J))}{\Delta Y_B} * \frac{\Delta X}{2} = \frac{H^{n+1}(I, J) - H^n(I, J)}{\Delta t}
 \end{aligned} \tag{9}$$

$$\begin{aligned}
 H^{n+1}(I, J) = & \Delta t * (h * T_I * (\Delta X + \Delta Y) / 2 + K_3 * T(I+1, J) * \Delta Y / (2 * \Delta X_R) \\
 & + K_4 * T(I, J+1) * \Delta X / (2 * \Delta Y_B) - (h * (\Delta X + \Delta Y) / 2 \\
 & + K_3 * \Delta Y / (2 * \Delta X_R) + K_4 * \Delta X / (2 * \Delta Y_B)) * T(I, J) + H^n(I, J)
 \end{aligned} \tag{10}$$

C. SPECIAL CONSIDERATIONS

1. Non-Uniform Grid Spacing

The welding operation presents a situation where a highly concentrated heat source is applied to a small region of a surface at a much lower temperature. This situation results in large temperature gradients in the vicinity of the torch. In order to increase the accuracy of the temperature values at any given location, the concentration of nodes in the affected area has been increased. In the horizontal direction, one-half of the nodes were located in the length directly under the heat source. The remaining half of the nodes were equally spaced over the distance from each side edge to the edge of the heat source. Similarly, one-half of the nodes were vertically positioned in the top 20 percent of the thickness.

The result is a fine grid mesh in the region directly under the heat source where the temperature changes from node to node are the greatest. As the distance from the heat source increases, the spacing between adjacent nodes increases, as seen in Figure 5.

2. Modeling the Welding Torch Arc

As seen in Figure 6, the heat source has been modeled as a Gaussian distribution. The rate at which energy is imparted from the torch to the surface is assumed to equal the voltage multiplied by the current multiplied by the welding efficiency.

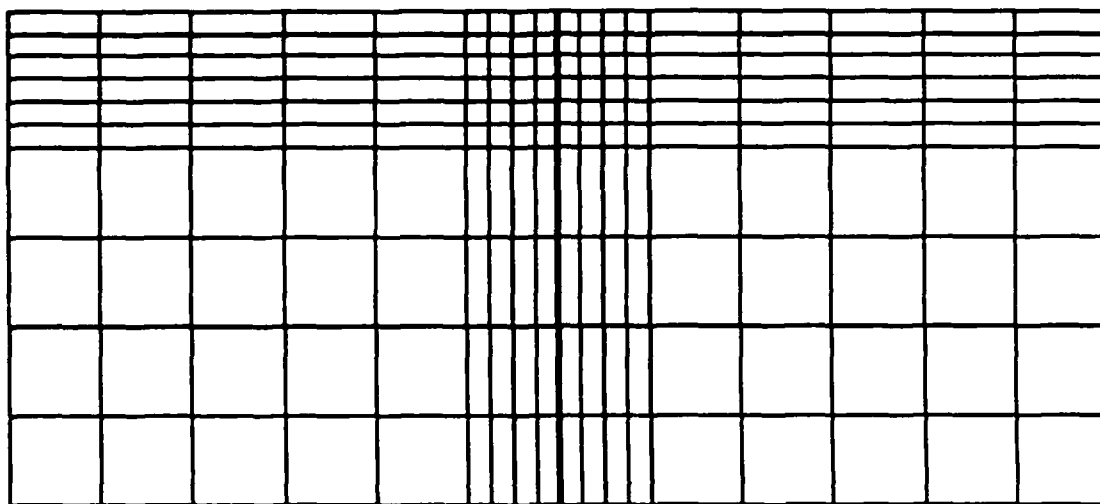


Figure 5. Non-Uniform Grid Illustration

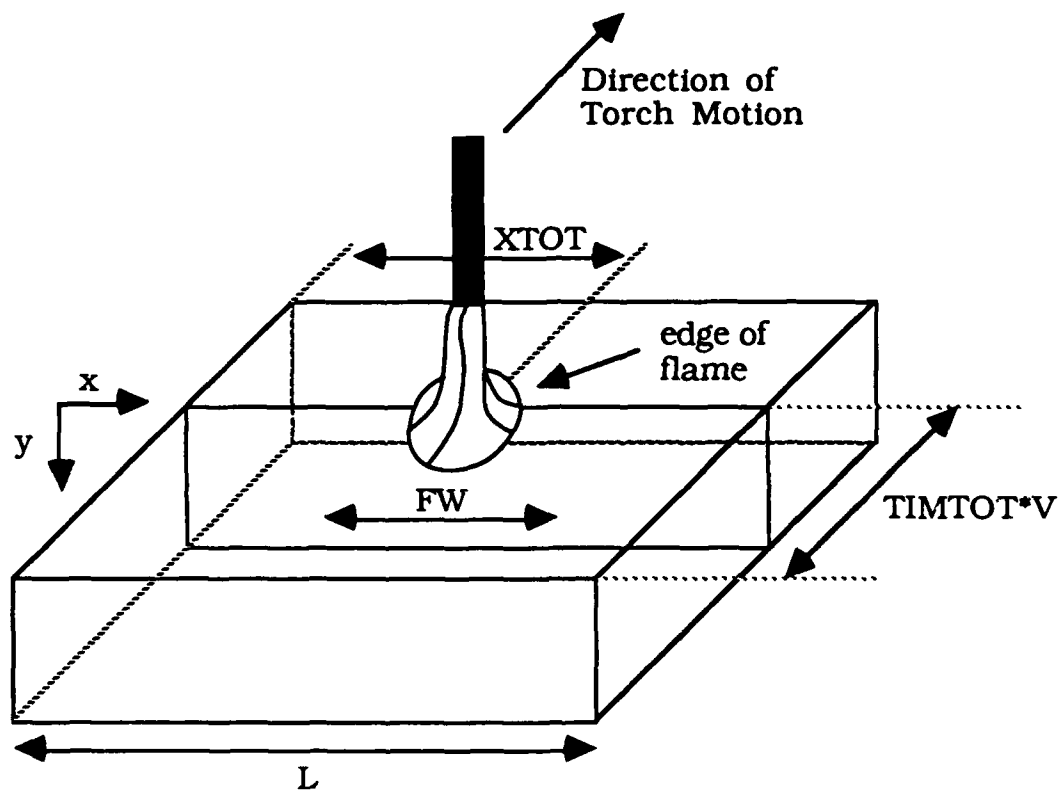


Figure 6. Welding Torch Arc

$$Q = \eta VI \quad (11)$$

where η , the welding efficiency, is an empirical factor to account for the energy losses from the arc and the weld pool surface.

Equation 11 also gives rise to a Gaussian distribution of the heat flux q'' . The maximum value of q'' occurs at the center line of the distribution. This peak flux value q''_0 was established such that the integral of the flux values over the area the torch covers (a circle of diameter FW, the flame width) is equal to ηVI .

$$q''_0 = \frac{C\eta VI}{\pi} \quad \text{where } C = -\frac{\ln(.01)}{\left(\frac{FW}{2}\right)^2} \quad (12)$$

The constant C was chosen such that the flux was reduced to a value of 1 percent of the center line value by the time it had reached the maximum distance from the center line (FW/2).

The model of the arc is designed to simulate the passage of the torch over a given cross-sectional plane. Equation 13 is the final equation taking both horizontal position and the passage of time into account.

$$q'' = q''_0 e^{-C(L/2 - XTOT)^2} e^{-C(FW/2 - (TIMTOT)(V))^2} \quad (13)$$

The first exponential term takes into account the horizontal location. The upper left-hand corner is always the origin. XTOT is the total distance traveled in the x direction. L/2 - XTOT represents the distance away from the center line. C is the same value as in equation

12. Far away from the center line, the argument of the exponential is a very large negative number, hence q'' approaches zero. As XTOT reaches the edge of the flame, q'' equals one percent of q''_0 . As XTOT reaches $L/2$, $q'' = q''_0$. The squaring of the distance allows the equation to decay as XTOT increases above $L/2$ in a mirror image of how it was built up.

The second exponential term is very similar to the first. However, this term accounts for the approach and passage of the torch over the cross-section of interest. $FW/2$ is the distance from the center line of the torch to the edge of the flame. $TIMTOT * V$ accounts for the distance that the torch has traveled from its initial starting point. The computations were started when the leading edge of the torch was $1/4 FW$ away from the cross-section of interest. Choosing this location allowed for observing the effects of the approach of the welding torch. As was the case in the horizontal direction, the flux value builds up to a maximum when the torch is directly over the cross-section of interest and decays off in a mirror image of the way it built up.

By multiplying the two exponential terms together, the true bell shape of the flux distribution is achieved.

D. SOLUTION PROCEDURE

This model of heat flow has been developed using the explicit technique. This implies that the enthalpy values for the new time level are calculated from known enthalpy values at the previous time level.

The enthalpy at each node was initialized based upon its control volume and the ambient temperature (293K). The enthalpy values for each node at time level $n + 1$ are determined using the equations in

Appendix A. The temperature at each node at time level $n + 1$ can then be determined through equation 14.

$$T^{n+1}(I,J) = \frac{H^{n+1}(I,J)}{\rho C_p \Delta X \Delta Y} \quad (14)$$

where ρ = density of material

$\Delta X \Delta Y$ = control volume term for 2D system

C_p = specific heat

The values for specific heat (C_p) are also temperature dependent. In order to use an explicit marching scheme, C_p was evaluated at temperatures calculated at time level n . Due to the small time steps used, the error due to this approximation is likely to be very small.

Once the temperature at a node has reached the melting temperature, equation 6 must be modified. The latent heat of fusion of the material must be accounted for. In order to get a correct temperature value once the material is molten, the latent heat of fusion must be subtracted from the enthalpy of the control volume, as seen in the following equations.

$$ENFUS = (\text{LATENT HEAT OF FUSION}) \rho \Delta X \Delta Y \quad (15)$$

$$ENMELT = (TMELT) C_p \rho \Delta X \Delta Y \quad (16)$$

For $H^{n+1}(I,J) > ENMELT + ENFUS$

$$T^{n+1}(I,J) = \frac{H^{n+1}(I,J) - ENFUS}{\rho C_p \Delta X \Delta Y} \quad (17)$$

For $ENMELT \leq H^{n+1}(I,J) < ENMELT + ENFUS$

$$T^{n+1} = TMELT \quad (18)$$

III. RESULTS

A. PARAMETERS

The model was run in tests of various combinations of the variable parameters. Test runs were made for two materials, steel and aluminum. The specific properties of the materials can be found in Appendix B [Ref. 11].

Because the model used the explicit method for solving the finite difference equations, computational stability was a matter of concern. For a two-dimensional problem, the Fourier number for an interior node must always be less than or equal to 0.25 to maintain stability [Ref. 12] (see equation 19). Expressions similar to equation 19 can be derived from the boundary nodes.

$$Fo = \frac{\alpha \Delta t}{(\Delta X)^2} = \frac{k \Delta t}{\rho C_p (\Delta X)^2} \leq \frac{1}{4} \quad (19)$$

The result of equation 19 is to tie the precision of location of any given node, the ΔX value, to the time step required to maintain stability. As the precision increases (ΔX decreases), the time step decreases by the square of the change in ΔX . This situation puts a premium on the minimum required accuracy in order to maintain reasonable time steps.

The parameters for the standard work pieces and torch settings were established as follows:

Width	0.35m	Voltage	28 Volts
Thickness	0.15m	Efficiency	0.80
Current	170 Amperes	Speed of Advance	2.54×10^{-3} m/sec

These dimensions and parameters were chosen to allow for comparison with results obtained from an instrumented steel slab with similar parameters performed by Kihara, et al., and described in Reference 1.

The first four computational runs for the two materials were made with varying spacing. The fifth run was made with an increased torch speed of advance. The sixth run was made with a reduced current. The seventh run was made with a smaller work piece.

B. DISCUSSION

The data from all runs can be found in Appendix D.

The first four sets of results show the effect of grid spacing upon the computations. In all cases, as the grid spacing became smaller, the temperature values are likely to become more accurate. The 40 x 40 grid spacing was taken as the optimum value since the highest temperature (center line value at time 8.8 seconds) was less than one percent different from the value obtained with a 50 x 50 grid spacing. The increase in accuracy obtained with the 50 x 50 grid spacing, though minimal, had a high cost in computational speed. The 50 x 50 grid required approximately twice the amount of time to run as did the 40 x 40 grid.

The data followed expected trends in that the steel heated up to a much higher temperature but the heat-affected zone was much smaller than for aluminum. This is appropriate because the thermal

diffusivity of aluminum ($\alpha_{Al} \approx 97 \times 10^6 \text{ m}^2/\text{sec}$) is approximately five times greater than the thermal diffusivity of steel ($\alpha_{Fe} \approx 18 \times 10^6 \text{ m}^2/\text{sec}$).

With current reduced by 10 percent from 170 Amps to 153 Amps and using a 41 x 41 grid, the maximum temperature rise achieved on the center line of the cross-section was reduced by approximately 10 percent in both the aluminum (11 percent) and steel (9.5 percent) samples. The depth of penetration of the molten region was also reduced as expected. Less energy being put into the samples resulted in less penetration and a lower peak temperature.

The increase in speed of advance of the torch by 10 percent from $2.54 \times 10^{-3} \text{ m/sec}$ to $2.794 \times 10^{-3} \text{ m/sec}$ resulted in a reduction of the increase in maximum center line temperature of approximately five percent. Again, the depth of penetration was reduced. In this case, the energy level was not reduced but it was not allowed to act on the cross-section as long. The net result was still less energy being input to the cross-section.

As a check of the model against experimental data, the 41 x 41 baseline grid was allowed to continue to run until 45 seconds had passed since the torch passed the cross-section (total time: 60.8 seconds). The center-line surface temperatures after the torch had passed were plotted against the data available from the instrumented slab experiments [Ref. 1]. The correlation between the model and the experimental data is good, especially since the material properties of

the experimental steel had to be approximated with data from the most similar alloy for which data were available (see Figure 7).

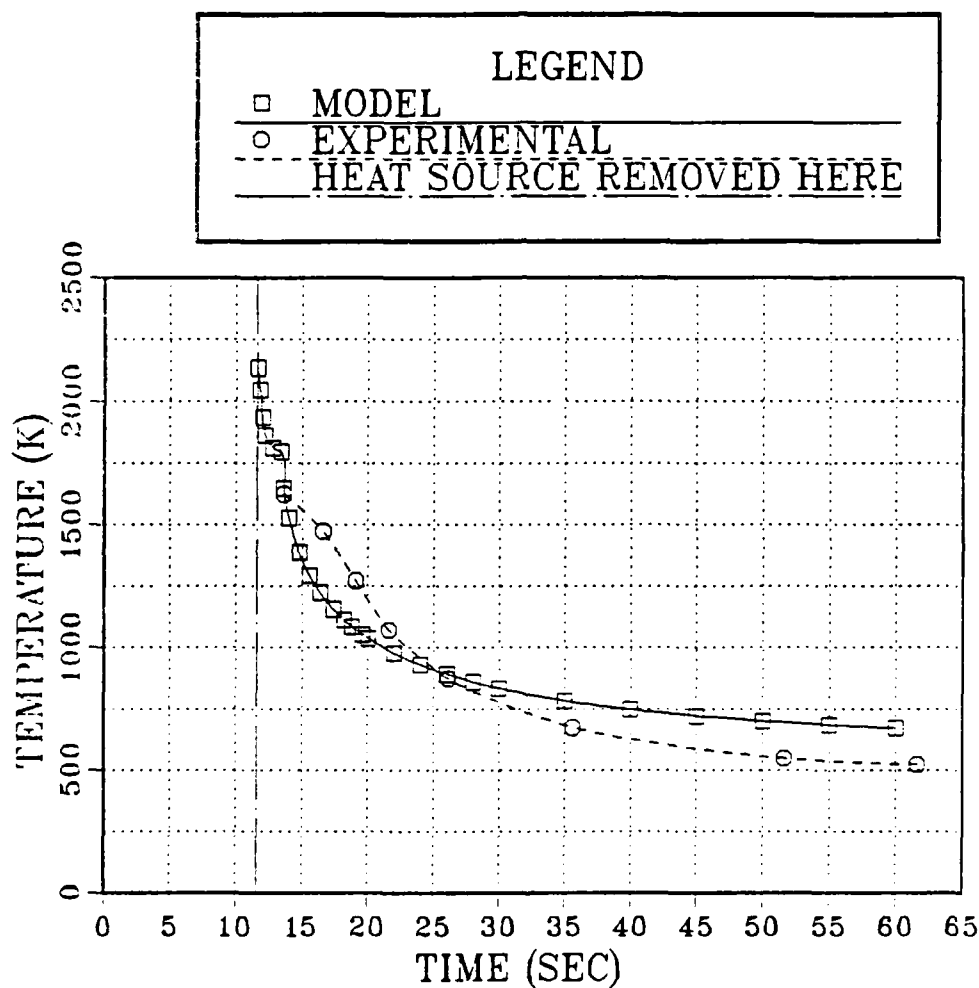


Figure 7. Comparison of Computational Results and Experimental Data From Kihara for Center-Line Surface Temperatures After the Heat Source Has Completely Passed the Center Line Surface Node

IV. CONCLUSIONS

The model developed here is an adequate simulation of the heat flow during fusion welding at locations far away from the ends of the work piece. Improvement can be made by addressing the convective heat transfer within the molten weld pool.

The model is based upon an explicit technique and hence is dependent upon the availability of a fast computer in order to handle small dimensions with good precision. To be practical for use on a mobile system, a fast, unconditionally stable model must be developed.

The model should be expanded to three dimensions in order to be reliable in all locations of the work piece, not just in the interior regions.

Actual experiments with instrumented work pieces should be performed to verify the data obtained from the model.

APPENDIX A

MODEL EQUATIONS

A. CONDUCTIVITY EQUATIONS

$$1. \quad K1 = k_{i-\frac{1}{2},j} = \frac{k_{i-1,j} * k_{i,j} * (\Delta XR + \Delta X)}{k_{i,j} * \Delta XR + k_{i-1,j} * \Delta X}$$

$$2. \quad K2 = k_{i,j-\frac{1}{2}} = \frac{k_{i,j-1} * k_{i,j} * (\Delta YT + \Delta Y)}{k_{i,j} * \Delta YT + k_{i,j-1} * \Delta Y}$$

$$3. \quad K3 = k_{i+\frac{1}{2},j} = \frac{k_{i+1,j} * k_{i,j} * (\Delta XR + \Delta X)}{k_{i,j} * \Delta XR + k_{i+1,j} * \Delta X}$$

$$4. \quad K4 = k_{i,j+\frac{1}{2}} = \frac{k_{i,j+1} * k_{i,j} * (\Delta YB + \Delta Y)}{k_{i,j} * \Delta YB + k_{i,j+1} * \Delta Y}$$

B. NODAL EQUATIONS

EN(I,J): enthalpy at node (i,j) from previous iteration [J/m]

EN1(I,J): enthalpy at node (i,j) for current iteration [J/m]

TIME: time step [sec]

H: convection (film) coefficient [W/m² K]

TI: ambient temperature [K]

Q: flux [W/m²]

1. NW Corner

$$\begin{aligned} \text{EN1(I,J)} = & \text{TIME} * ((\Delta X + \Delta Y) * H * T_{I/2} + K3 * T(I+1,J) \\ & * \Delta Y / (2 * \Delta X_R) + K4 * T(I,J+1) * \Delta X / (2 * \Delta Y_B) \\ & - ((\Delta X + \Delta Y) * H / 2 + K3 * \Delta Y / (2 * \Delta X_R) + K4 \\ & * \Delta X / (2 * \Delta Y_B)) * T(I,J)) + \text{EN(I,J)} \end{aligned}$$

2. SW Corner

$$\begin{aligned} \text{EN1(I,J)} = & \text{TIME} * ((\Delta X + \Delta Y) * H * T_{I/2} + K3 * T(I+1,J) \\ & * \Delta Y / (2 * \Delta X_R) + K2 * T(I,J-1) * \Delta X / (2 * \Delta Y_T) \\ & - ((\Delta X + \Delta Y) * H / 2 + K2 * \Delta Y / (2 * \Delta X_R) + K2 \\ & * \Delta X / (2 * \Delta Y_T)) * T(I,J)) + \text{EN(I,J)} \end{aligned}$$

3. Left Wall (Not Corners)

$$\begin{aligned} \text{EN1(I,J)} = & \text{TIME} * (\Delta Y * H * T_I + K3 * T(I+1,J) * \Delta Y / \Delta X_R \\ & + K2 * T(I,J-1) * \Delta X / (2 * \Delta Y_T) + K4 * T(I,J+1) \\ & * \Delta X / (2 * \Delta Y_B) - (H * \Delta Y + K3 * \Delta Y / \Delta X_R + K2 \\ & * \Delta X / (2 * \Delta Y_T) + K4 * \Delta X / (2 * \Delta Y_B)) * T(I,J)) + \text{EN(I,J)} \end{aligned}$$

4. NE Corner

$$\begin{aligned} \text{EN1(I,J)} = & \text{TIME} * ((\Delta X + \Delta Y) * H * T_{I/2} + K1 * T(I-1,J) \\ & * \Delta Y / (2 * \Delta XL) + K4 * T(I,J+1) * \Delta X / (2 * \Delta YB) \\ & - ((\Delta X + \Delta Y) * H / 2 + K1 * \Delta Y / (2 * \Delta XL) + K4 \\ & * \Delta X / (2 * \Delta YB)) * T(I,J)) + \text{EN(I,J)} \end{aligned}$$

5. Top Wall—Flux (Not Corners)

$$\begin{aligned} \text{EN1(I,J)} = & \text{TIME} * (Q * \Delta X + K1 * T(I-1,J) * \Delta Y / (2 * \Delta XL) \\ & + K3 * T(I+1,J) * \Delta Y / (2 * \Delta XR) + K4 * T(I,J+1) \\ & * \Delta X / \Delta YB - (K1 * \Delta Y / (2 * \Delta XL) + K3 * \Delta Y / (2 * \Delta XR) \\ & + K4 * \Delta X / \Delta YB) * T(I,J)) + \text{EN(I,J)} \end{aligned}$$

6. Top Wall—Flux/No Flux Interface

$$\begin{aligned} \text{EN1(I,J)} = & \text{TIME} * (Q * \Delta X / 2 + \Delta X * H * T_{I/2} + K1 * T(I-1,J) \\ & * \Delta Y / (2 * \Delta XL) + K3 * T(I+1,J) * \Delta Y / (2 * \Delta XR) \\ & + K4 * T(I,J+1) * \Delta X / \Delta YB - (H * \Delta X / 2 + K1 \\ & * \Delta Y / (2 * \Delta XL) + K3 * \Delta Y / (2 * \Delta XR) + K4 \\ & * \Delta X / \Delta YB) * T(I,J)) + \text{EN(I,J)} \end{aligned}$$

7. Top Wall—No Flux

$$\begin{aligned} EN1(I,J) = & TIME * (\Delta X * H * TI + K1 * T(I-1,J) \\ & * \Delta Y / (2 * \Delta XL) + K3 * T(I+1,J) * \Delta Y / (2 * \Delta XR) \\ & + K4 * T(I,J+1) * \Delta X / \Delta YB - (\Delta X * H + K1 \\ & * \Delta Y / (2 * \Delta XL) + K3 * \Delta Y / (2 * \Delta XR) + K4 \\ & * \Delta X / \Delta YB) * T(I,J)) + EN(I,J) \end{aligned}$$

8. SE Corner

$$\begin{aligned} EN1(I,J) = & TIME * ((\Delta X + \Delta Y) * H * TI / 2 + K1 * T(I-1,J) \\ & * \Delta Y / (2 * \Delta XL) + K2 * T(I,J-1) * \Delta X / (2 * \Delta YT) \\ & - ((\Delta X + \Delta Y) * H / 2 + K1 * \Delta Y / (2 * \Delta XL) + K2 \\ & * \Delta X / (2 * \Delta YT)) * T(I,J)) + EN(I,J) \end{aligned}$$

9. Right Wall (Not Corners)

$$\begin{aligned} EN1(I,J) = & TIME * (\Delta Y * H * TI + K1 * T(I-1,J) * \Delta Y / \Delta XL \\ & + K2 * T(I,J-1) * \Delta X / (2 * \Delta YT) + K4 * T(I,J+1) \\ & * \Delta X / (2 * \Delta YB) - (\Delta Y * H + K1 * \Delta Y / \Delta XL + K2 \\ & * \Delta X / (2 * \Delta YT) + K4 * \Delta X / (2 * \Delta YB)) * T(I,J)) + EN(I,J) \end{aligned}$$

10. Bottom Wall (Not Corners)

$$\begin{aligned} \text{EN1(I,J)} = & \text{TIME} * (\Delta X * H * T_I + K1 * T(I-1,J) * \Delta Y / (2 * \Delta XL) \\ & + K3 * T(I+1,J) * \Delta Y / \Delta XR + K2 * T(I,J-1) * \Delta X / \Delta YT \\ & - (\Delta X * H + K1 * \Delta Y / (2 * \Delta XL) + K3 * \Delta Y / (2 * \Delta XR) \\ & + K2 * \Delta X / \Delta YT) * T(I,J)) + \text{EN(I,J)} \end{aligned}$$

11. Interior Points

$$\begin{aligned} \text{EN1(I,J)} = & \text{TIME} * (K1 * T(I-1,J) * \Delta Y / \Delta XL + K3 * T(I+1,J) \\ & * \Delta Y / \Delta XR + K2 * T(I,J-1) * \Delta X / \Delta YT + K4 \\ & * T(I,J+1) * \Delta X / \Delta YB - (K1 * \Delta Y / \Delta XL + K3 * \Delta Y / \Delta XR \\ & + K2 * \Delta X / \Delta YT + K4 * \Delta X / \Delta YB) * T(I,J)) + \text{EN(I,J)} \end{aligned}$$

APPENDIX B MATERIAL DATA

1. Aluminum

99.996% pure
Melting Temperature = 933.5K
LHF = 3.98×10^5 J/kg

a. Conductivity

Temperature [K]	Conductivity [W/m K]
273.2	239
373.2	234
473.2	228
573.3	221
673.2	215
773.2	208
873.2	201
973.2	103
1073.2	121

Approximated by:

$$K = 248.918398 - .02075127 T - 6.324 \times 10^{-5} T^2 + 2.78 \times 10^{-8} T^3$$

[W/m K]

b. Specific Heat

Temperature [K]	C _p [cal/g K]
373.0	2.2832×10^{-1}
473.0	2.3795×10^{-1}
573.0	2.4759×10^{-1}
673.0	2.5760×10^{-1}
773.0	2.6723×10^{-1}
873.0	2.7687×10^{-1}

Approximated by:

$$C_p = 803.1932 + .4071 T \text{ [J/kg K]}$$

2. Steel

Alloy: .23C 1.50 Mn .12 Si

Melting Temperature = 1810 K

LHF = 2.473×10^5 J/kg

a. Conductivity

Temperature [°K]	Conductivity [W/m K]
273.2	46.0
323.2	46.0
373.2	46.0
423.2	45.6

Approximated by:

$$K = 46.7358 - .0024 T \text{ [W/m K]}$$

b. Specific Heat

Alloy: .13C .61 Mn .2 Si

Temperature [K]	C_p [cal/g K]
273	.1039
293	.1061
323	.1109
373	.1180
423	.1221
473	.1260
523	.1291
573	.1331
623	.1381
673	.1429
723	.1501
773	.1582
823	.1671
873	.1802
923	.1953

Temperature [K]	C _p [cal/g K]
973	.2151
1013	.2414
1036	.2916
1053	.2130
1073	.1991
1113	.1871
1141	.1821
1179	.1570
1223	.1561
1273	.1570

Approximated by:

$$C_p = 418.458 + .2115 T \text{ [J/kg K]}$$

The numerical data was obtained from Reference 11.

APPENDIX C COMPUTER PROGRAM OF MODEL

*

* THIS PROGRAM CALCULATES THE TEMPERATURE
 * DISTRIBUTION IN A FLAT PLATE WHICH IS
 * EXPOSED TO CONVECTIVE AND RADIATIVE
 * LOSSES ON ALL SIDES AND HAS A GAUSSIAN
 * DISTRIBUTION HEAT SOURCE PASS DOWN THE
 * CENTERLINE OF THE PLATE.

*

```

  DIMENSION T(051,051),EN1(051,051),OUTPT(6,051),
& TEST(6),EN(051,051),T9(051,051),S(051,051),
& KMELT(051,051)
  REAL*8 DX,DY,F,K,L,W,INTVL,Q,A1,B1,C1,D1,TIME,RHO,C,
& R,Z9,ERC,K9,T,T9,EN1,EN,OUTPT,TEST,S,T1,K1,K2,K3,
& 4,ENMELT,TMELT,FW,Q0,V,C2,KMELT,EFF,VOLT,CURR,
& QTOT10,HC,ENFUS,TIMTOT,FACTOR,DXL,DNR,DYT,DYB,
& NTOT,DX1,DX2
  INTEGER I,J,FINISH,CNT,BAR,N,Z,FLUX1,FLUX2,WF,II,
& J1,FLAG
  COMMON II,J1,A1,B1,C1,D1,T,K1,K2,K3,K4,KMELT,DXL,
& DNR,DYT,DYB
  OPEN(UNIT = 1,FILE = 'OUTPT')
  A1 = 46.7358
  B1 = -.002409148
  C1 = 0
  D1 = 0

```

*

*****SET BAR PARAMETERS*****

*

L = 0.26250D0
W = 0.11250D0
EFF = 0.8D0
VOLT = 028.D0
CURR = 170.D0
RHO = 7.85E + 03
HC = 9.782
FACTOR = 1.0
N = 030
TIMORG = .02000D0
TIME = TIMORG
FW = 2.000E-02
V = 2.540E-03
TMELT = 1810.D0

*

*

FLUX1 = NINT(.5*N + 1) - INT(.25*N)
FLUX2 = NINT(.5*N + 1) + INT(.25*N)
QTOT = 0
WRITE(*,*) FLUX1,FLUX2
C2 = -LOG(.01) / (FW * 2)**2
Q0 = LIT * VOLT * CURR * C2 * 3.141593
TI = 293.D0
DO 100 J = 1, N + 1
DO 105 I = 1, N + 1
KMELT(I,J) = 1.D0

***** NW CORNER

IF ((J.EQ.1).AND.(I.EQ.1)) THEN
S(I,J) = .25D0

***** SW CORNER

ELSE IF ((J.EQ.N + 1).AND.(I.EQ.1)) THEN

```

      S(I,J) = .25D0
*****      LEFT WALL (NOT CORNERS)
      ELSE IF (I.EQ.1) THEN
        S(I,J) = .5D0
*****      NE CORNER
      ELSE IF ((J.EQ.1).AND.(I.EQ.N+1)) THEN
        S(I,J) = .25D0
*****      TOP WALL (NOT CORNERS)
      ELSE IF ((J.EQ.1).AND.(I.GT.FLUX1).AND.(I.LT.FLUX2))
& THEN
        S(I,J) = .5D0
*****      SE CORNER
      ELSE IF ((J.EQ.N+1).AND.(I.EQ.N+1)) THEN
        S(I,J) = .25D0
*****      RIGHT WALL (NOT CORNERS)
      ELSE IF (I.EQ.N+1) THEN
        S(I,J) = .5D0
*****      BOTTOM WALL (NOT CORNERS)
      ELSE IF (J.EQ.N+1) THEN
        S(I,J) = .5D0
*****      INTERIOR POINTS
      ELSE
        S(I,J) = 1.D0
      END IF
      T(I,J) = 293.D0
      IF ((I.GT.FLUX1).AND.(I.LT.FLUX2)) THEN
        DX = FW (FLUX2-FLUX1)
        DX1 = DX
      ELSE IF ((I.EQ.FLUX1).OR.(I.EQ.FLUX2)) THEN
        DX = (FW (FLUX2-FLUX1) + (L-FW) (N+FLUX1-FLUX2)) / 2
      ELSE
        DX = (L-FW) (N+FLUX1-FLUX2)
        DX2 = DX
      END IF

```

```

IF (J.LT.NINT(.5*(N+1))) THEN
  DY=0.2*W.NINT(.5*(N+1))
ELSE IF (J.EQ.NINT(.5*(N+1))) THEN
  DY=(.2*W.NINT(.5*(N+1))+.8*W.(N-NINT(.5*(N+1)))) 2
ELSE
  DY=0.8*W.(N-NINT(.5*(N+1)))
END IF
EN(I,J)=7.85E+03*480.428*293*DX*DY*S(I,J)
T9(I,J)=293
105 CONTINUE
100 CONTINUE
109 FORMAT(IX,21F5.2)
TIMTOT=0
CNT=0
110 CNT=CNT+1
TIMTOT=TIMTOT+TIME
DO 200 J=1,N+1
  XTOT=0
  DO 205 I=1,N+1
    T9(I,J)=T(I,J)
    IF ((I.GT.FLUX1).AND.(I.LT.FLUX2)) THEN
      DX=FW (FLUX2-FLUX1)
      IF (I-1.EQ.FLUX1) THEN
        DXL=((L-FW) (N+FLUX1-FLUX2)+FW (FLUX2-FLUX1)) 2
        DXR=DX
      ELSE IF (I+1.EQ.FLUX2) THEN
        DXL=DX
        DXR=((L-FW) (N+FLUX1-FLUX2)+FW (FLUX2-FLUX1)) 2
      ELSE
        DXL=DX
        DXR=DX
      END IF
    ELSE IF (I.EQ.FLUX1) THEN
      DX=(FW (FLUX2-FLUX1)+(L-FW) (N+FLUX1-FLUX2)) 2

```

```

DXL = (L-FW) (N + FLUX1-FLUX2)
DXR = FW (FLUX2-FLUX1)
ELSE IF (I.EQ.FLUX2) THEN
  DX = (FW (FLUX2-FLUX1) + (L-FW) (N + FLUX1-FLUX2)) / 2
  DXL = FW (FLUX2-FLUX1)
  DXR = (L-FW) (N + FLUX1-FLUX2)
ELSE
  DX = (L-FW) (N + FLUX1-FLUX2)
  IF (I + 1.EQ.FLUX1) THEN
    DXL = DX
    DXR = (FW (FLUX2-FLUX1) + (L-FW) (N + FLUX1-FLUX2)) / 2
  ELSE IF (I - 1.EQ.FLUX2) THEN
    DXL = (FW (FLUX2-FLUX1) + (L-FW) (N + FLUX1-FLUX2)) / 2
    DXR = DX
  ELSE
    DXL = DX
    DXR = DX
  END IF
END IF
IF (J.LT.NINT(.5*(N+1))) THEN
  DY = 0.2*W NINT(.5*(N+1))
  IF (J - 1.EQ.NINT(.5*(N+1))) THEN
    DYT = DY
    DYB = (.8*W (N-NINT(.5*(N+1))) + .2*W
& NINT(.5*(N+1))) / 2
  ELSE
    DYT = DY
    DYB = DY
  END IF
ELSE IF (J.EQ.NINT(.5*(N+1))) THEN
  DY = (.2*W NINT(.5*(N+1)) + .8*W (N-NINT(.5*(N+1)))) / 2
  DYT = .2*W NINT(.5*(N+1))
  DYB = .8*W (N-NINT(.5*(N+1)))
ELSE

```

```

      DY=0.8*W*(N-NINT(.5*(N+1)))
      DYT=DY
      DYB=DY
END IF
I1=I
J1=J
K1=0
K2=0
K3=0
K4=0
H=HC+4.0*5.67E-08*.5*T(I,J)**3
*****      NW CORNER
      IF ((J.EQ.1).AND.(I.EQ.1)) THEN
        CALL COND3
        CALL COND4
        EN1(I,J)=TIME*((DX+DY)*H*TI 2+K3*T(I+1,J)*
&  DY (2*DNR) +K4*T(I,J+1)*DX (2*DYB)-((DX+DY)
&  *H 2+K3*DY (2*DNR)+K4*DX (2*DYB))
&  *T(I,J))+EN(I,J)
*****      SW CORNER
      ELSE IF ((J.EQ.N+1).AND.(I.EQ.1)) THEN
        CALL COND2
        CALL COND3
        EN1(I,J)=TIME*((DX+DY)*H*TI 2+K3*T(I+1,J)*
&  DY (2*DNR)+K2*T(I,J-1)*DX (2*DYT)-((DX+DY)
&  *H 2+K3*DY (2*DNR)+K2*DX (2*DYT))
&  *T(I,J))+EN(I,J)
*****      LEFT WALL (NOT CORNERS)
      ELSE IF (I.EQ.1) THEN
        CALL COND2
        CALL COND3
        CALL COND4
        EN1(I,J)=TIME*(DY*H*TI+K3*T(I+1,J)*DY DNR
&  +K2*T(I,J-1)*DX (2*DYT)+K4*T(I,J+1)

```

```

& *DX (2*DYB)-(H*DY+K3*DY DXR+K2*DX (2*DYT)
& +K4*DX (2*DYB))*T(I,J))+EN(I,J)
*****      NE CORNER
ELSE IF ((J.EQ.1).AND.(I.EQ.N+1)) THEN
  CALL COND1
  CALL COND4
  EN1(I,J)=TIME*((DX+DY)*H*TI2+K1*T(I-1,J)
& *DY (2*DXL)+K4*T(I,J+1)*DX (2*DYB)-((DX+DY)
& *H2+K1*DY (2*DXL)+K4*DX (2*DYB))
& *T(I,J))+EN(I,J)
*****      TOP WALL-FLUX (NOT CORNERS)
ELSE IF ((J.EQ.1).AND.(I.GT.FLUX1).AND.(I.LT.FLUX2))
& THEN
  IF (EXP(-C2*(L2-XTOT)**2).LT.0.01) GO TO 999
  IF (EXP(-C2*(2.00*FW2-TIMTOT*V)**2).LT.0.01) GO TO
& 999
  CALL COND1
  CALL COND3
  CALL COND4
  Q=Q0*EXP(-C2*(L2-XTOT)**2)*EXP(-C2*(2.00*FW2
& -TIMTOT*V)**2)
  EN1(I,J)=TIME*(Q*DX+K1*T(I-1,J)*DY (2*DXL)
& +K3*T(I+1,J)*DY (2*DXR)+K4*T(I,J+1)*DX DYB-(K1
& *DY (2*DXL)+K3*DY (2*DXR)+K4*DX DYB)
& *T(I,J))+EN(I,J)
*****      TOP WALL-FLUX NO FLUX INTFC
ELSE IF ((J.EQ.1).AND.((I.EQ.FLUX1).OR.
& (I.EQ.FLUX2)).AND.(FLUX1.NE.FLUX2)) THEN
  IF (EXP(-C2*(L2-XTOT)**2).LT.0.01) GO TO 999
  IF (EXP(-C2*(2.00*FW2-TIMTOT*V)**2).LT.0.01) GO TO
& 999
  CALL COND1
  CALL COND3
  CALL COND4

```

```

      Q=Q0*EXP(-C2*(L/2-XTOT)**2)*EXP(-C2*(2.00*FW/2
& -TIMTOT*V)**2)
      EN1(I,J)=TIME*(Q*DX/2+DX*H*TI/2+K1*T(I-1,J)
& *DY/(2*DXL)+K3*T(I+1,J)*DY/(2*DXR)+K4*T(I,J+1)
& *DX/DYB-(H*DX/2+K1*DY/(2*DXL)+K3*DY/(2*DXR)
& +K4*DX/DYB)*T(I,J))+EN(I,J)
      ELSE IF (J.EQ.1).AND.((I.EQ.FLUX1).OR.
& (I.EQ.FLUX2)).AND.(FLUX1.EQ.FLUX2)) THEN
      IF (EXP(-C2*(L/2-XTOT)**2).LT.0.01) GO TO 999
      IF (EXP(-C2*(2.00*FW/2-TIMTOT*V)**2).LT.0.01) GO TO
& 999
      CALL COND1
      CALL COND3
      CALL COND4
      Q=Q0*EXP(-C2*(L/2-XTOT)**2)*EXP(-C2*(2.00*FW/2
& -TIMTOT*V)**2)
      EN1(I,J)=TIME*(Q*DX+K1*T(I-1,J)*DY/(2*DXL)
& +K3*T(I+1,J)*DY/(2*DXR)+K4*T(I,J+1)*DX/DYB-(H*DX/2
& +K1*DY/(2*DXL)+K3*DY/(2*DXR)+K4*DX/DYB)
& *T(I,J))+EN(I,J)
*****      TOP WALL-NO FLUX
      ELSE IF ((J.EQ.1).AND.((I.LT.FLUX1).OR.(I.GT.FLUX2)))
& THEN
999      CALL COND1
      CALL COND3
      CALL COND4
      EN1(I,J)=TIME*(DX*H*TI+K1*T(I-1,J)*DY/(2*DXL)
& +K3*T(I+1,J)*DY/(2*DXR)+K4*T(I,J+1)*DX/DYB-(DX*H
& +K1*DY/(2*DXL)+K3*DY/(2*DXR)+K4*DX/DYB)
& *T(I,J))+EN(I,J)
*****      SE CORNER
      ELSE IF ((J.EQ.N+1).AND.(I.EQ.N+1)) THEN
      CALL COND1
      CALL COND2

```

```

      EN1(I,J)= TIME*((DX+DY)*H*TI 2+ K1*T(I-1,J)
&  *DY (2*DXL)+ K2*T(I,J-1)*DX (2*DYT)-((DX+DY)
&  *H 2+ K1*DY (2*DXL)+ K2*DX (2*DYT))
&  *T(I,J))+ EN(I,J)
*****          RIGHT WALL (NOT CORNERS)
      ELSE IF (I.EQ.N+1) THEN
        CALL COND1
        CALL COND2
        CALL COND4
        EN1(I,J)= TIME*(DY*H*TI+ K1*T(I-1,J)*DY DXL
&  + K2*T(I,J-1)*DX (2*DYT)+ K4*T(I,J+1)*DX (2*DYB)
&  -(DY*H+ K1*DY DXL+ K2*DX (2*DYT)+ K4*DX (2*DYB))
&  *T(I,J))+ EN(I,J)
*****          BOTTOM WALL
      ELSE IF (J.EQ.N+1) THEN
        CALL COND1
        CALL COND2
        CALL COND3
        EN1(I,J)= TIME*(DX*H*TI+ K1*T(I-1,J)*DY (2*DXL)
&  + K3*T(I+1,J)*DY (2*DXR)+ K2*T(I,J-1)*DX DYT
&  -(DX*H+ K1*DY (2*DXL)+ K3*DY (2*DXR)+ K2*DX DYT)
&  *T(I,J))+ EN(I,J)
*****          INTERIOR POINTS
      ELSE
        CALL COND1
        CALL COND2
        CALL COND3
        CALL COND4
        EN1(I,J)= TIME*(K1*T(I-1,J)*DY DXL+ K3*T(I+1,J)
&  *DY DXR+ K2*T(I,J-1)*DX DYT+ K4*T(I,J+1)*DX DYB
&  -(K1*DY DXL+ K3*DY DXR+ K2*DX DYT+ K4*DX DYB)
&  *T(I,J))+ EN(I,J)
      END IF
      IF ((I.LE.FLUX1).AND.(I.LT.FLUX2)) THEN

```



```

      XTOT = XTOT + DX1
    ELSE
      XTOT = XTOT + DX2
    END IF
205  CONTINUE
200  CONTINUE
    FLAG = 0
    DO 300 I = 1, N + 1
      DO 305 J = 1, N + 1
        IF ((I.GT.FLUX1).AND.(I.LT.FLUX2)) THEN
          DX = FW (FLUX2-FLUX1)
        ELSE IF ((I.EQ.FLUX1).OR.(I.EQ.FLUX2)) THEN
          DX = (FW (FLUX2-FLUX1) + (L-FW) (N + FLUX1-FLUX2)) 2
        ELSE
          DX = (L-FW) (N + FLUX1-FLUX2)
        END IF
        IF (J.LT.NINT(.5*(N + 1))) THEN
          DY = 0.2*W NINT(.5*(N + 1))
        ELSE IF (J.EQ.NINT(.5*(N + 1))) THEN
          DY = (.2*W NINT(.5*(N + 1)) + .8*W (N-NINT(.5*(N + 1)))) 2
        ELSE
          DY = 0.8*W (N-NINT(.5*(N + 1)))
        END IF
        C = 418.485 + 0.2115*T(I,J)
        ENMELT = TMELT*(418.458 + .2115*TMELT)*RHO*DX*DY*S(I,J)
        IF (ENI(I,J).GT.ENMELT) THEN
          ENFUS = 247300*RHO*DX*DY
          IF (ENI(I,J).GT.(ENMELT + ENFUS)) THEN
            T(I,J) = (ENI(I,J)-ENFUS) (RHO*C*DX*DY*S(I,J))
            KMELT(I,J) = FACTOR
            FLAG = FLAG + 1
          ELSE
            T(I,J) = TMELT
          C      KMELT(I,J) = 1.D0

```

```

      END IF
    ELSE
      T(I,J)= EN1(I,J) (RHO*C*DX*DY*S(I,J))
    END IF
    IF (FLAG.EQ.0) THEN
      TIME= TIMORG
    ELSE
      TIME= TIMORG FACTOR
    END IF
    EN(I,J)= EN1(I,J)
305  CONTINUE
300  CONTINUE
415  FORMAT(1X,26F5.0)
C415  FORMAT(3F4.0,35F5.0,3F4.0)
420  IF(CNT.EQ.1) GO TO 422
      IF (CNT.NE.INT(CNT/0010)*0010) GO TO 400
C  WRITE(1,*)
422  WRITE(*,*) CNT
421  FORMAT(1X,F8.1,1X,F8.1,1X,F8.1,1X,F8.1,1X,F8.1)
      WRITE(1,421) TIMTOT
      DO 500 J= 1,N+1
        WRITE(1,415) (T(I,J)-293,I= 1,16)
500  CONTINUE
      WRITE(1,*)
C400  CONTINUE
400  T9(I,J)= T(I,J)
      IF (TIMTOT.LT.15.6) GO TO 110
601  CONTINUE
602  FORMAT(1X,11A11)
      CLOSE(1)
C  WRITE(*,*) QTOT
      END
*****  SUBROUTINES FOR VALUES OF K
      SUBROUTINE CONDI

```

```

DIMENSION T(051,051),KMELT(051,051)
REAL*8 A1,B1,C1,D1,A,B,T,K1,K2,K3,K4,KMELT,
& DXL,DXR,DYT,DTB
COMMON I1,J1,A1,B1,C1,D1,T,K1,K2,K3,K4,KMELT,DXL,
& DXR,DYT,DYB
INTEGER I1,J1
A = A1 + B1*T(I1-1,J1) + C1*T(I1-1,J1)**2 + D1*T(I1-1,J1)**3
B = A1 + B1*T(I1,J1) + C1*T(I1,J1)**2 + D1*T(I1,J1)**3
K1 = A*B*(DXL + DXR)/(DXL*B + DXR*A)*KMELT(I1,J1)
END

SUBROUTINE COND2
DIMENSION T(051,051),KMELT(051,051)
REAL*8 A1,B1,C1,D1,A,B,T,K1,K2,K3,K4,KMELT,DXL,
& DXR,DYT,DTB
COMMON I1,J1,A1,B1,C1,D1,T,K1,K2,K3,K4,KMELT,DXL,
& DXR,DYT,DYB
INTEGER I1,J1
A = A1 + B1*T(I1,J1-1) + C1*T(I1,J1-1)**2 + D1*T(I1,J1-1)**3
B = A1 + B1*T(I1,J1) + C1*T(I1,J1)**2 + D1*T(I1,J1)**3
K2 = A*B*(DYT + DYB)/(DYT*B + DYB*A)*KMELT(I1,J1)
END

SUBROUTINE COND3
DIMENSION T(051,051),KMELT(051,051)
REAL*8 A1,B1,C1,D1,A,B,T,K1,K2,K3,K4,KMELT,DXL,
& DXR,DYT,DTB
COMMON I1,J1,A1,B1,C1,D1,T,K1,K2,K3,K4,KMELT,DXL,
& DXR,DYT,DYB
INTEGER I1,J1
A = A1 + B1*T(I1+1,J1) + C1*T(I1+1,J1)**2 + D1*T(I1+1,J1)**3
B = A1 + B1*T(I1,J1) + C1*T(I1,J1)**2 + D1*T(I1,J1)**3
K3 = A*B*(DXL + DXR)/(DXL*A + DXR*B)*KMELT(I1,J1)
END

SUBROUTINE COND4
DIMENSION T(051,051),KMELT(051,051)

```

```

REAL*8 A1,B1,C1,D1,A,B,T,K1,K2,K3,K4,KMELT,DXL,
& DXR,DYT,DTB
COMMON I1,J1,A1,B1,C1,D1,T,K1,K2,K3,K4,KMELT,DXL,
& DXR,DYT,DYB
INTEGER I1,J1
A = A1 + B1*T(I1,J1 + 1) + C1*T(I1,J1 + 1)**2 + D1*T(I1,J1 + 1)**3
B = A1 + B1*T(I1,J1) + C1*T(I1,J1)**2 + D1*T(I1,J1)**3
K4 = A*B*(DYT + DYB) (DYT*A + DYB*B)*KMELT(I1,J1)
END

```

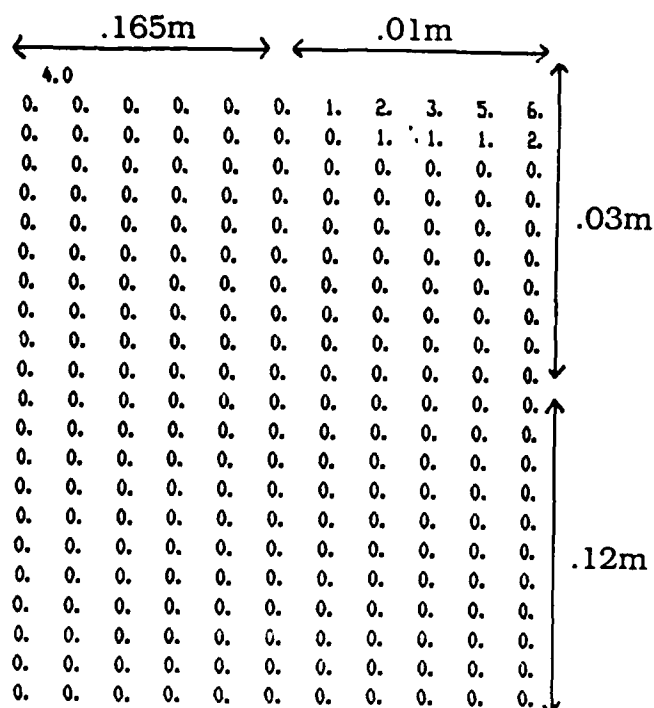
APPENDIX D

DATA

The data is presented in the following format.

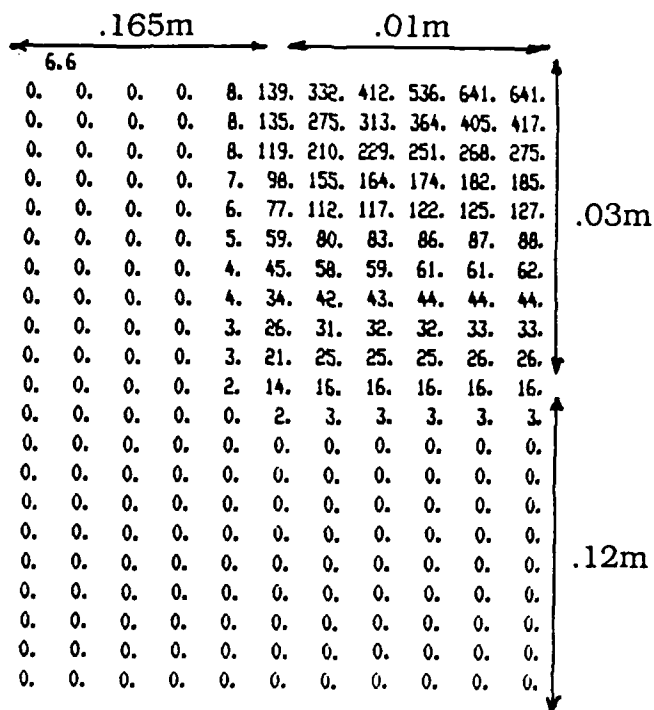
- Number on top line to the left is time (seconds) after start of data run.
- Data is presented as a temperature increase (K) over initial temperature (293K)
- Only the left half of the cross-section is presented; the right half is a mirror image for all runs presented. (The left column of data corresponds to the left edge of the cross-section. The right column of the data is at the center line of the cross-section.)
- One-half of the vertical nodes are concentrated in the top 20 percent of the thickness and one-half of the horizontal nodes are concentrated in the first 0.01 m out from the center line.
- Each data run has four time sheets presented:

1) initial heating phase	~4.0 sec
2) initial onset of molten conditions	~6.6 sec
3) maximum heat input	~8.8 sec
4) end of run (torch completely past cross-section)	15.6 sec
- Molten condition for aluminum: +641K
- Molten condition for steel: +1571K



AL
 Width: .35m
 Thickness: .15m
 Current: 170A
 Voltage: 28V
 Welding Eff.: $\eta = .8$
 Torch Speed: $v = 2.54 \text{ mm/sec}$

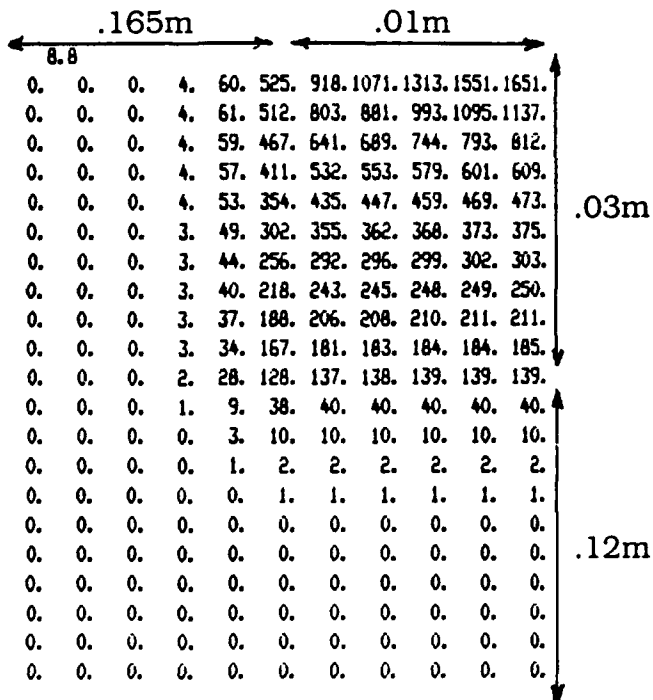
21 x 21



AL

Width: .35m
 Thickness: .15m
 Current: 170A
 Voltage: 28V
 Welding Eff.: $\eta = .8$
 Torch Speed: $v = 2.54 \text{ mm/sec}$

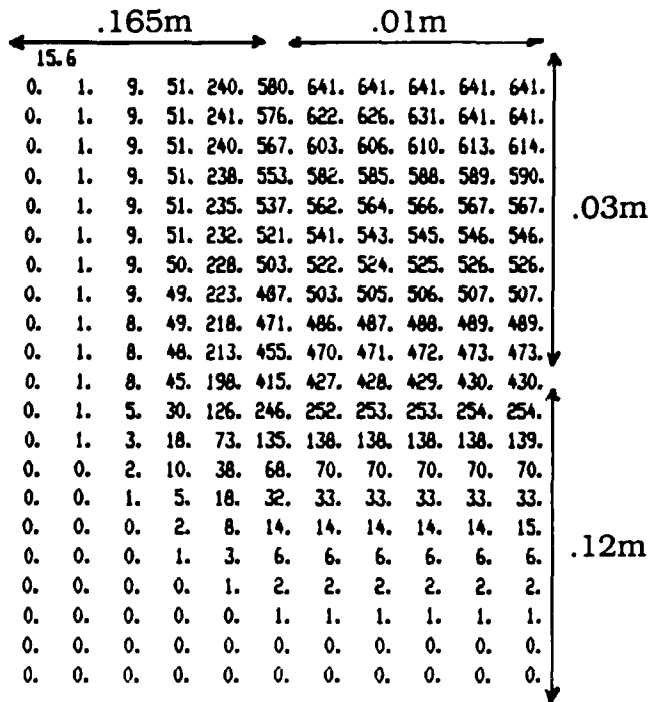
21 x 21



AL

Width: .35m
Thickness: .15m
Current: 170A
Voltage: 28V
Welding Eff.: $\eta = .8$
Torch Speed: $v = 2.54 \text{ mm/sec}$

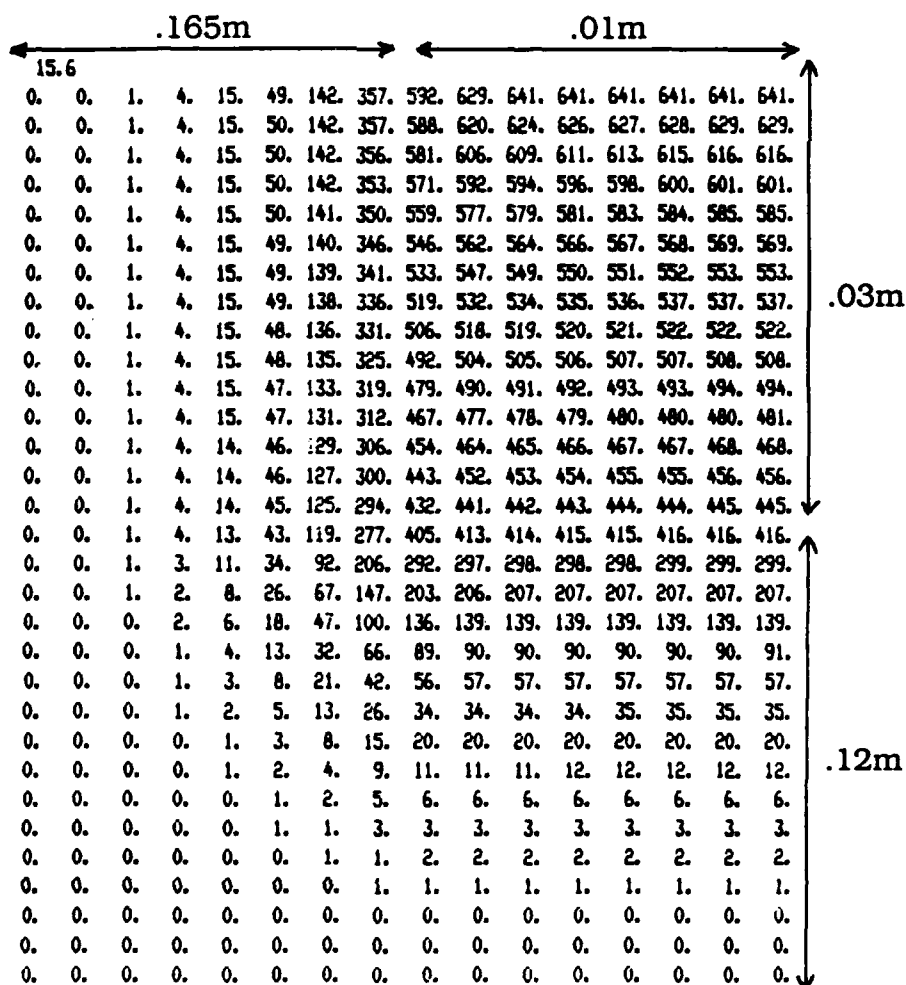
21 x 21



AL

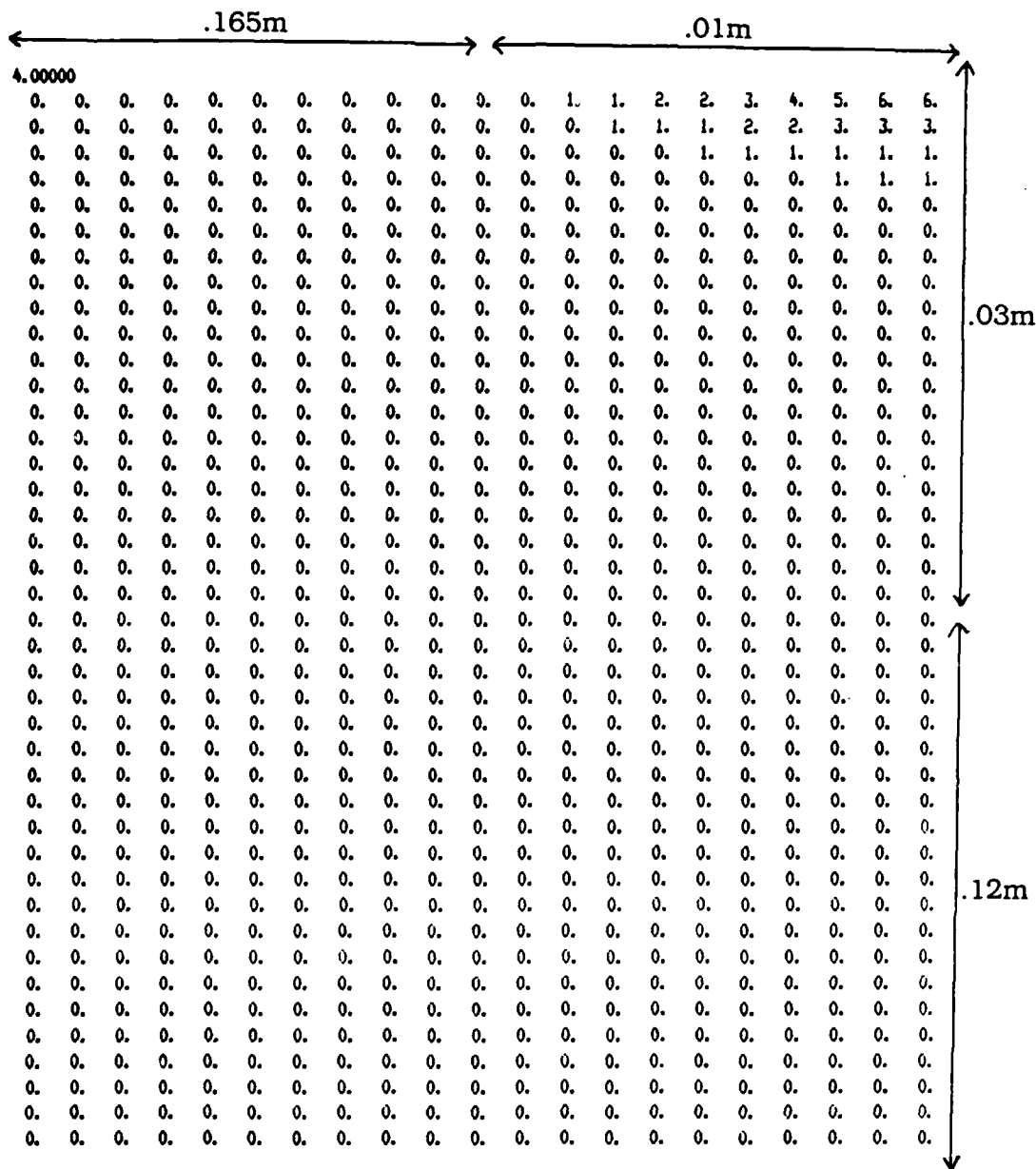
Width: .35m
 Thickness: .15m
 Current: 170A
 Voltage: 28V
 Welding Eff.: $\eta = .8$
 Torch Speed: $v = 2.54 \text{ mm/sec}$

21 x 21



Width: .35m
 Thickness: .15m
 Current: 170A
 Voltage: 28V
 Welding Eff.: $\eta = .8$
 Torch Speed: $v = 2.54 \text{ mm/sec}$

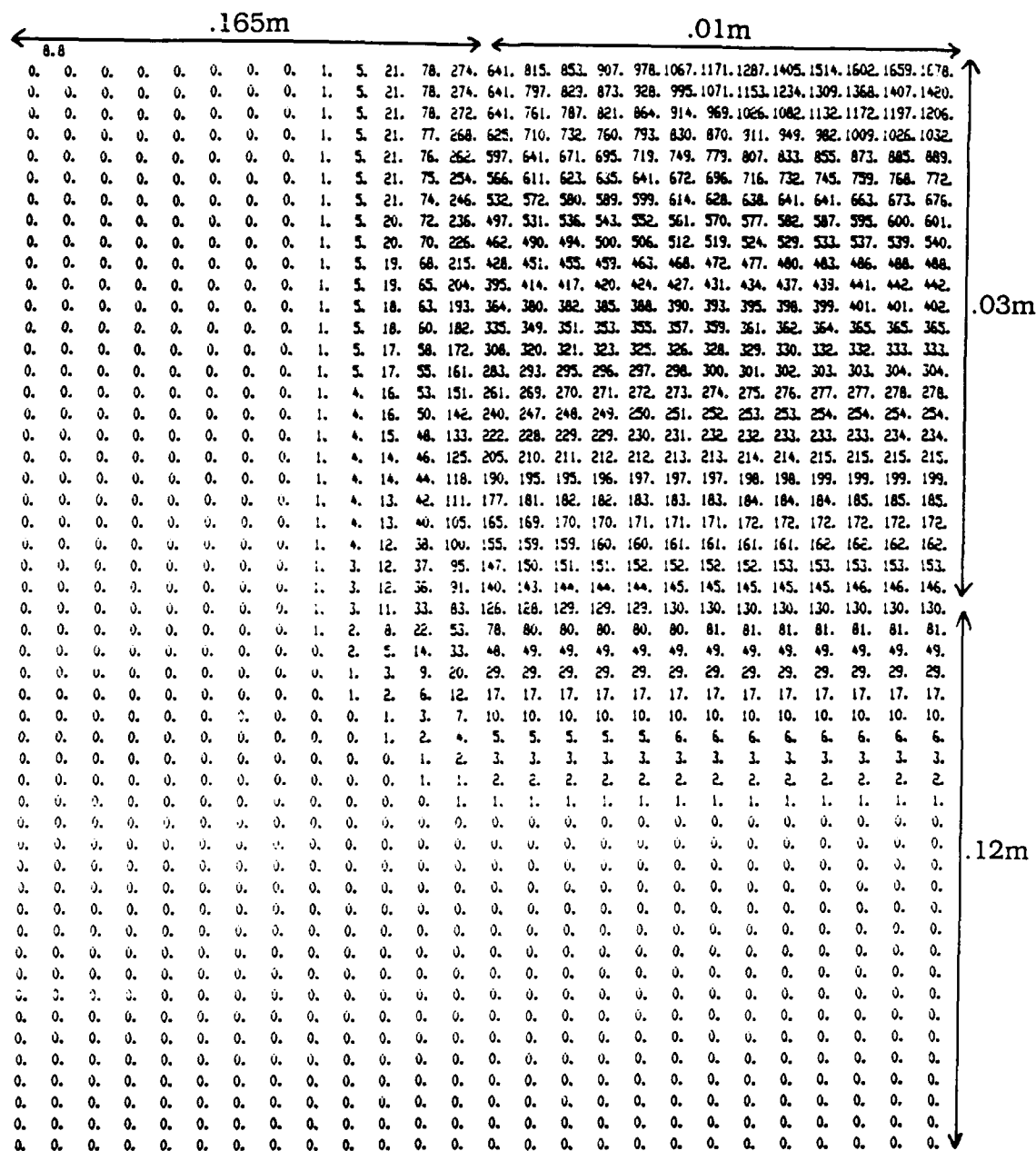
31 x 31



AL

Thickness / Current: .15m 170A
 Width / Welding Eff.: .35m $\eta = .8$
 Voltage / Torch Speed: 28V $v = 2.54 \text{ mm/sec}$

41 x 41



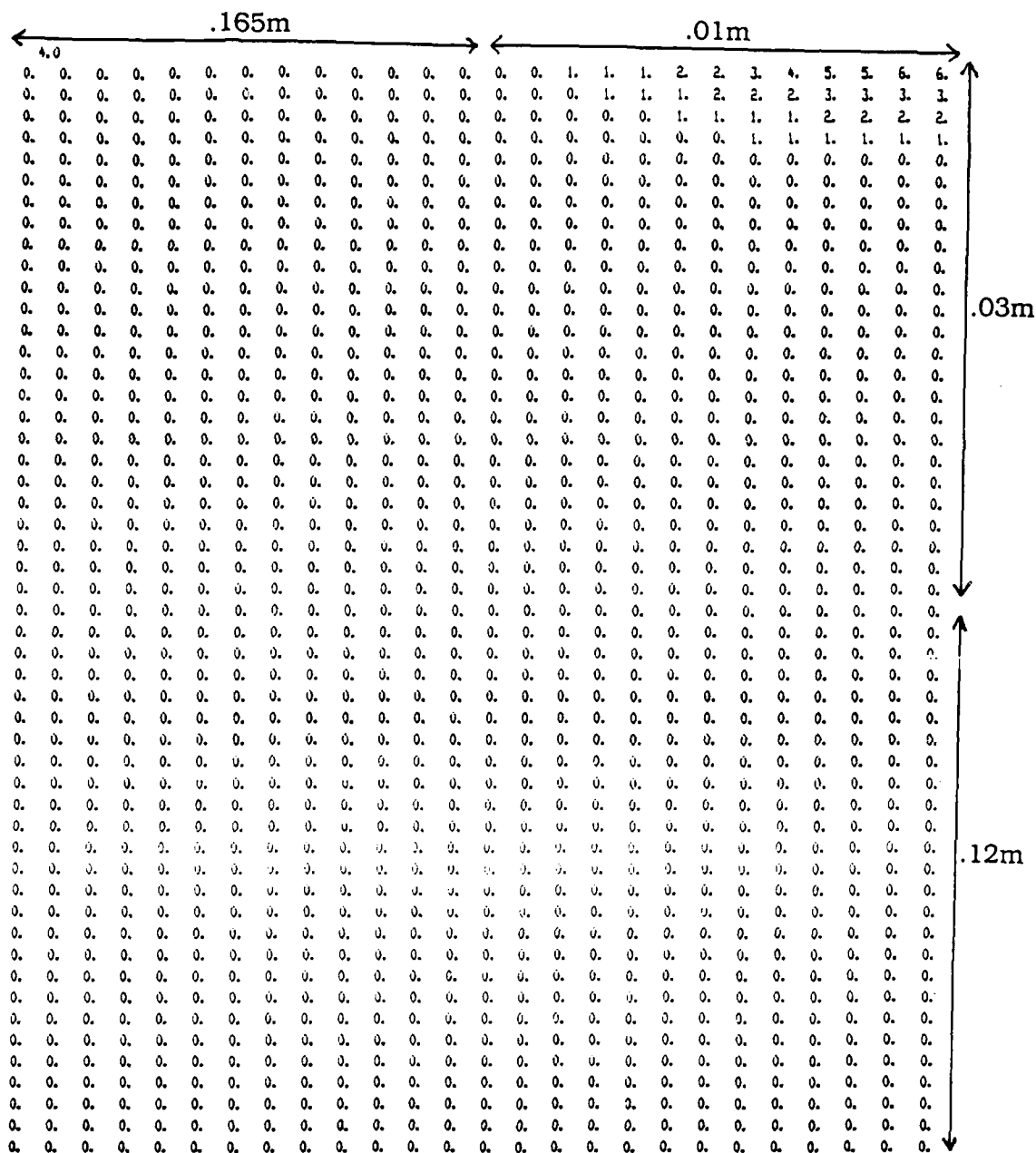
AL

Width / Voltage: .35m 28V

Thickness / Welding Eff.: .15m $\eta = .8$

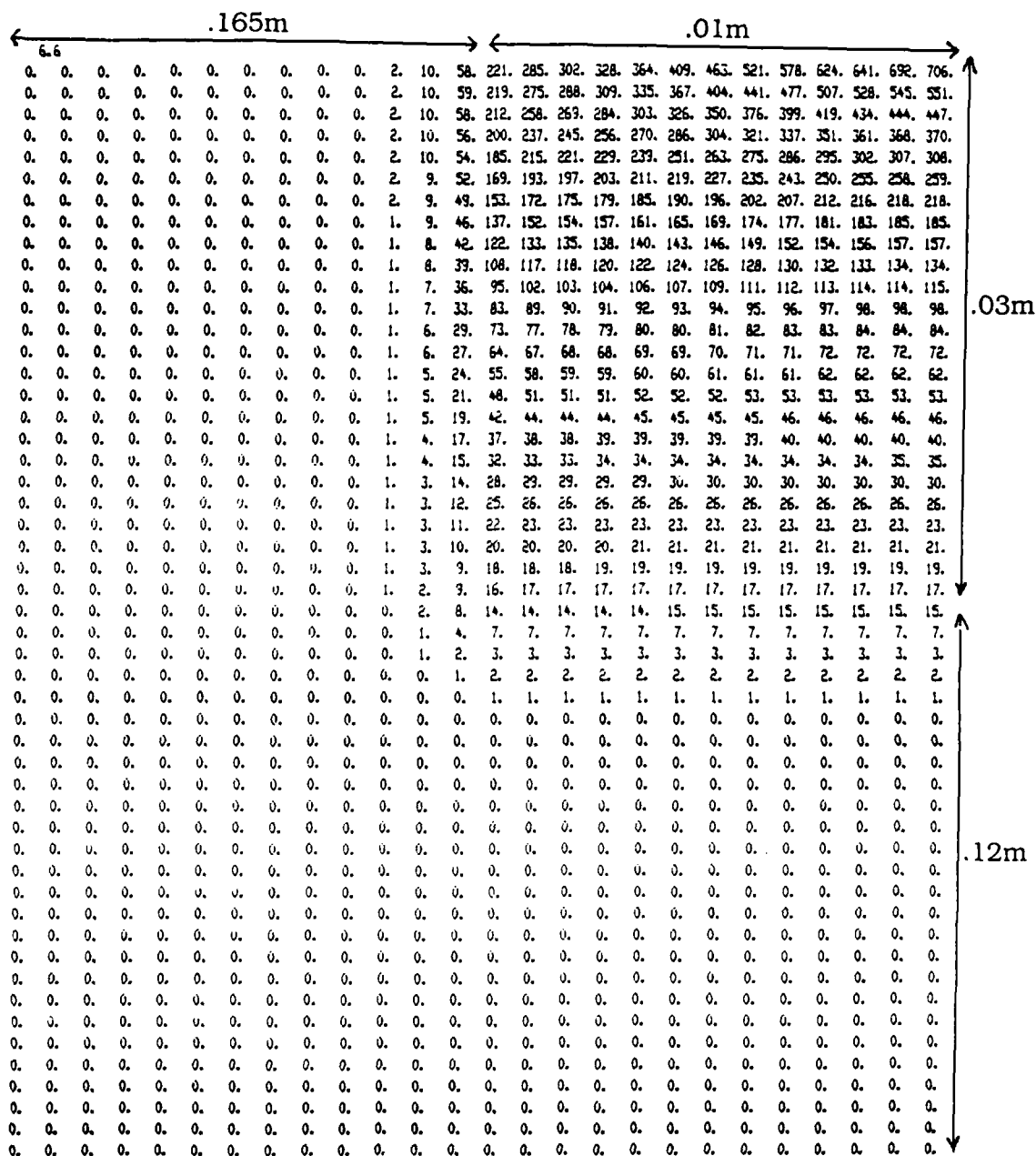
Current / Torch Speed: 170A $v = 2.54 \text{ mm/sec}$

51 x 51

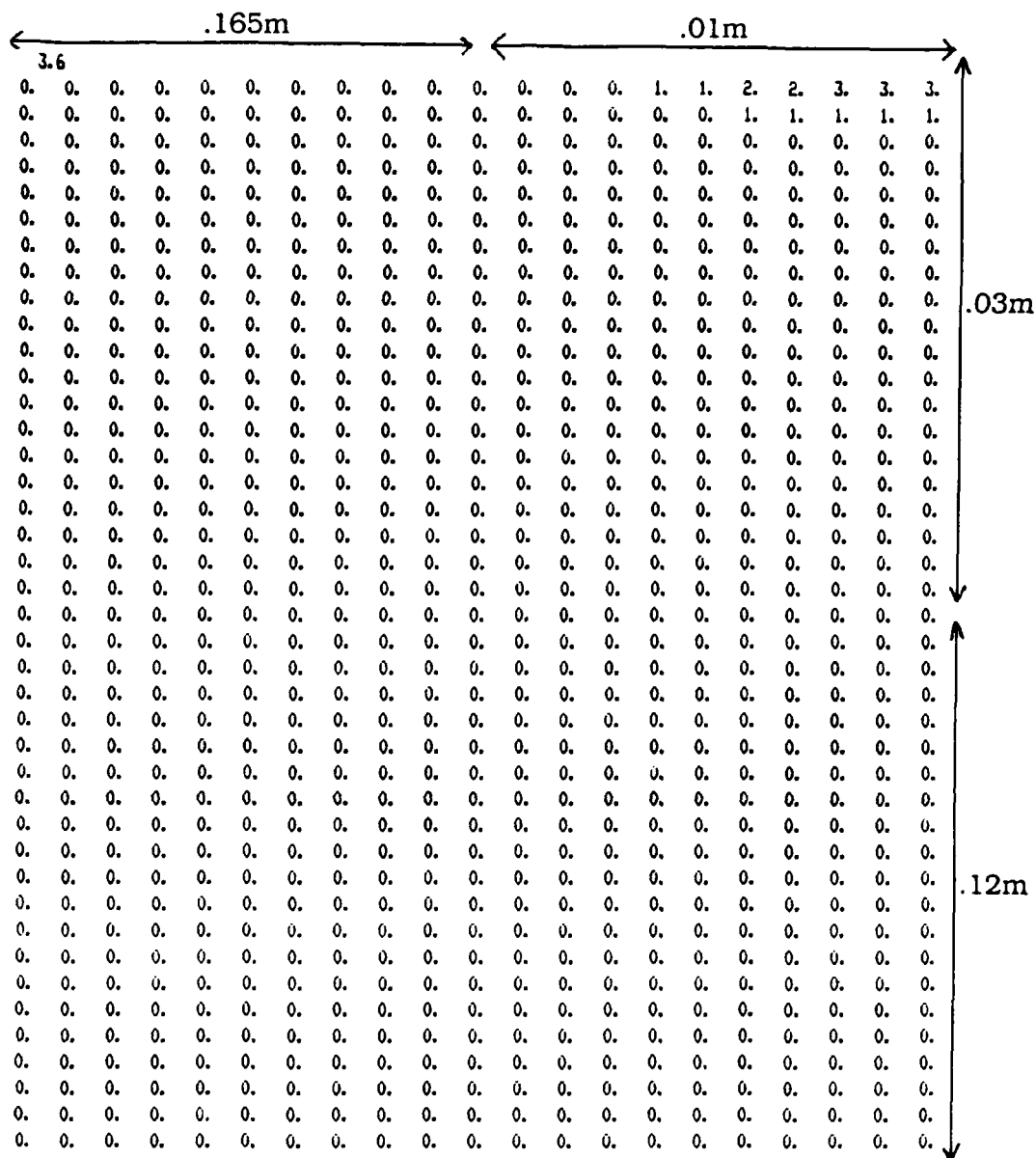


AL

Width / Voltage: .35m 28V
 Thickness / Welding Eff.: .15m $\eta = .8$
 Current / Torch Speed: 170A $v = 2.54 \text{ mm/sec}$
 51 x 51



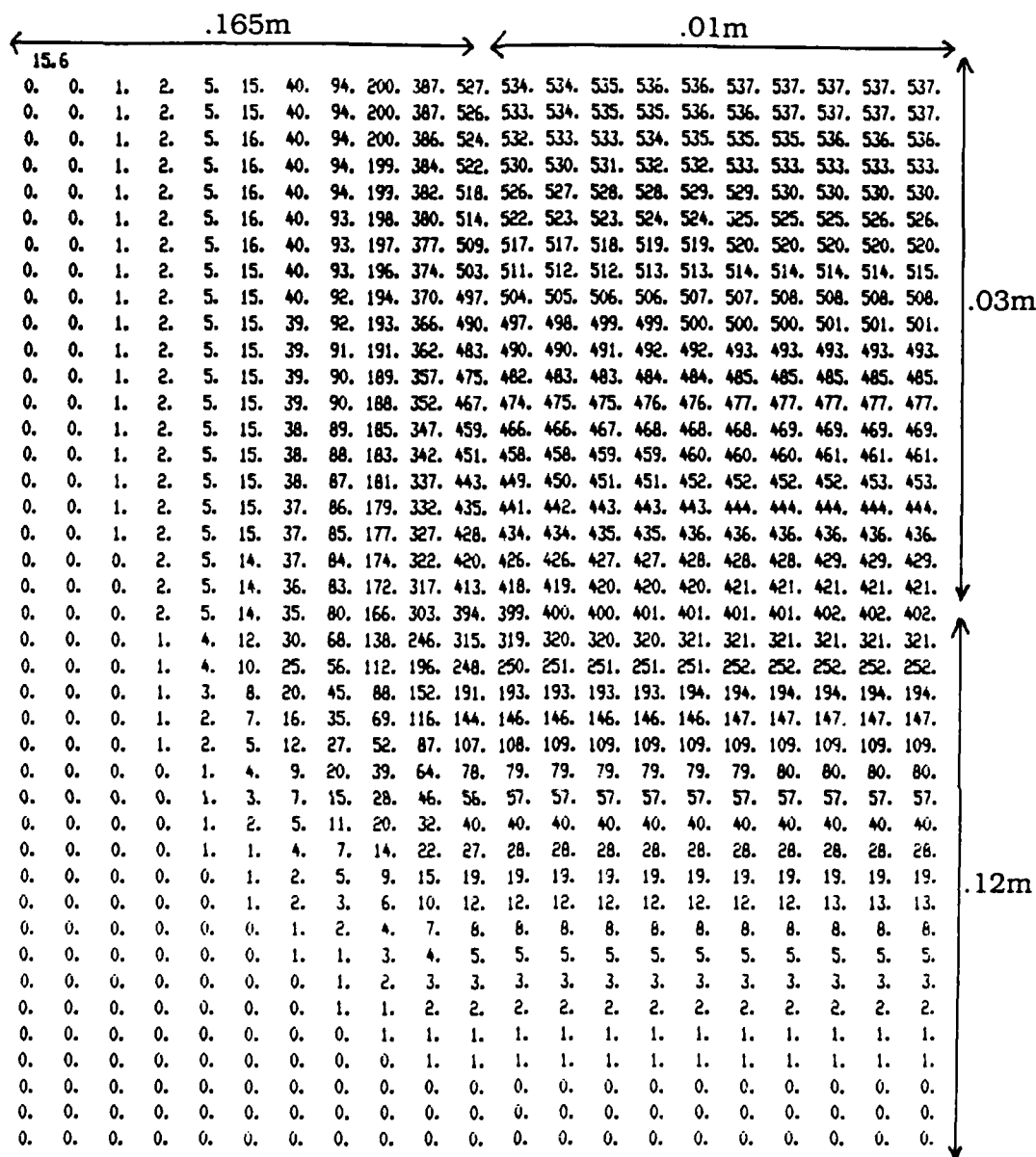
Width / Voltage: .35m 28V
 Thickness / Welding Eff.: .15m $\eta = .8$
 Current / Torch Speed: 170A $v = 2.54 \text{ mm/sec}$
 51 x 51



AL

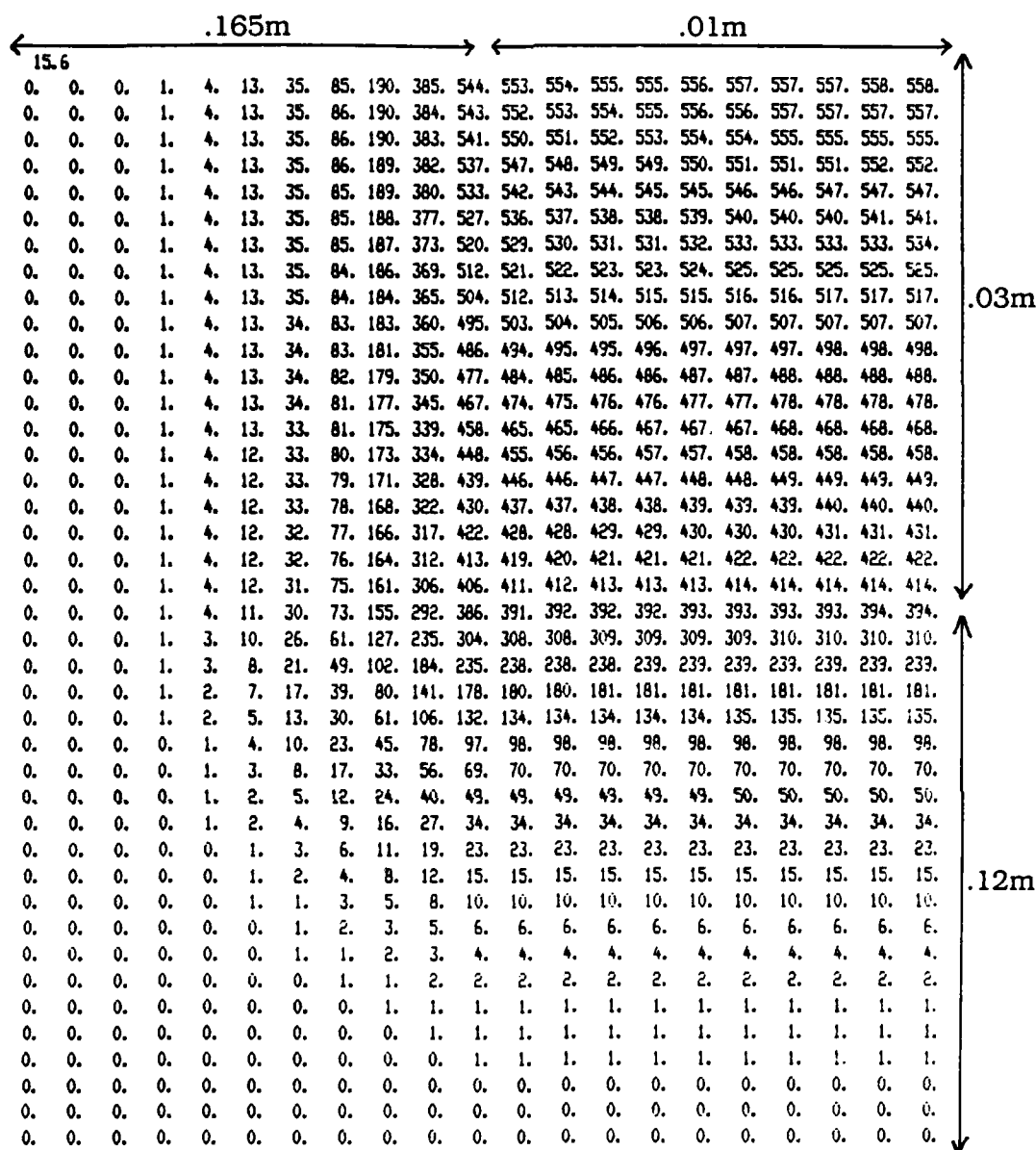
Width / Voltage: .35m 28V
 Thickness / Welding Eff.: .15m $\eta = .8$
 Current / Torch Speed: 170A $v = 2.794 \text{ mm/sec}$

40 x 40



Width / Voltage: .35m 28V
 Thickness / Welding Eff.: .15m $\eta = .8$
 Current / Torch Speed: 170A $v = 2.794 \text{ mm/sec}$

41 x 41



AL

Width / Voltage: .35m 28V
 Thickness / Welding Eff.: .15m $\eta = .8$
 Current / Torch Speed: 153A $v = 2.54 \text{ mm/sec}$

41 x 41



				.1213m				.01m							
8.8															
0.	0.	0.	0.	2.	10.	47.	202.	582.	764.	842.	970.	1138.	1318.	1458.	1511.
0.	0.	0.	0.	2.	10.	47.	202.	577.	736.	796.	888.	1000.	1114.	1200.	1232.
0.	0.	0.	0.	2.	10.	47.	200.	560.	687.	728.	795.	871.	945.	1000.	1020.
0.	0.	0.	0.	2.	10.	47.	197.	534.	629.	641.	703.	753.	807.	844.	857.
0.	0.	0.	0.	2.	10.	46.	192.	504.	582.	599.	627.	641.	694.	723.	732.
0.	0.	0.	0.	2.	10.	45.	187.	472.	536.	550.	569.	587.	612.	629.	635.
0.	0.	0.	0.	2.	10.	45.	180.	439.	491.	503.	516.	530.	544.	554.	558.
0.	0.	0.	0.	2.	10.	44.	173.	407.	449.	458.	468.	478.	487.	493.	495.
0.	0.	0.	0.	2.	10.	43.	166.	377.	411.	417.	425.	432.	438.	442.	443.
0.	0.	0.	0.	2.	9.	41.	158.	348.	376.	381.	387.	392.	396.	399.	400.
0.	0.	0.	0.	2.	9.	40.	151.	322.	346.	350.	354.	358.	361.	363.	363.
0.	0.	0.	0.	2.	9.	39.	144.	300.	319.	323.	326.	329.	331.	332.	333.
0.	0.	0.	0.	2.	9.	38.	138.	280.	297.	299.	302.	304.	306.	307.	308.
0.	0.	0.	0.	2.	9.	37.	132.	263.	278.	280.	283.	285.	286.	287.	287.
0.	0.	0.	0.	2.	8.	36.	127.	250.	263.	265.	267.	269.	270.	271.	271.
0.	0.	0.	0.	2.	8.	33.	115.	220.	231.	233.	235.	236.	237.	238.	238.
0.	0.	0.	0.	1.	5.	22.	70.	124.	129.	130.	131.	131.	132.	132.	132.
0.	0.	0.	0.	1.	3.	13.	41.	68.	70.	71.	71.	71.	71.	72.	72.
0.	0.	0.	0.	0.	2.	8.	22.	36.	37.	37.	37.	38.	38.	38.	38.
0.	0.	0.	0.	0.	1.	4.	12.	18.	19.	19.	19.	19.	19.	19.	19.
0.	0.	0.	0.	0.	1.	2.	6.	9.	9.	9.	9.	9.	9.	9.	10.
0.	0.	0.	0.	0.	0.	1.	3.	4.	4.	4.	5.	5.	5.	5.	5.
0.	0.	0.	0.	0.	0.	1.	1.	2.	2.	2.	2.	2.	2.	2.	2.
0.	0.	0.	0.	0.	0.	0.	1.	1.	1.	1.	1.	1.	1.	1.	1.
0.	0.	0.	0.	0.	0.	0.	0.	0.	0.	0.	0.	0.	0.	0.	0.
0.	0.	0.	0.	0.	0.	0.	0.	0.	0.	0.	0.	0.	0.	0.	0.
0.	0.	0.	0.	0.	0.	0.	0.	0.	0.	0.	0.	0.	0.	0.	0.
0.	0.	0.	0.	0.	0.	0.	0.	0.	0.	0.	0.	0.	0.	0.	0.
0.	0.	0.	0.	0.	0.	0.	0.	0.	0.	0.	0.	0.	0.	0.	0.
0.	0.	0.	0.	0.	0.	0.	0.	0.	0.	0.	0.	0.	0.	0.	0.
0.	0.	0.	0.	0.	0.	0.	0.	0.	0.	0.	0.	0.	0.	0.	0.
0.	0.	0.	0.	0.	0.	0.	0.	0.	0.	0.	0.	0.	0.	0.	0.
0.	0.	0.	0.	0.	0.	0.	0.	0.	0.	0.	0.	0.	0.	0.	0.
0.	0.	0.	0.	0.	0.	0.	0.	0.	0.	0.	0.	0.	0.	0.	0.

.0225m

.09m

AL

Thickness: .1125m
Width: .2625m
Current: 170A
Voltage: 28V
Welding Eff.: $\eta = .8$
Torch Speed: $v = 2.54 \text{ mm/sec}$

31 x 31

← .1213m →															← .01m →														
15.6																													
2.	3.	8.	20.	49.	108.	220.	414.	577.	599.	605.	611.	621.	641.	641.	641.	641.	641.	641.	641.	641.	641.	641.	641.	641.	641.	641.	641.	641.	641.
2.	3.	8.	20.	49.	108.	220.	414.	576.	598.	603.	609.	617.	625.	627.	628.	628.	628.	628.	628.	628.	628.	628.	628.	628.	628.	628.	628.	628.	628.
2.	3.	8.	20.	49.	108.	220.	413.	574.	594.	599.	604.	609.	613.	616.	616.	616.	616.	616.	616.	616.	616.	616.	616.	616.	616.	616.	616.	616.	616.
2.	3.	8.	20.	49.	108.	220.	412.	570.	589.	593.	597.	600.	603.	605.	606.	606.	606.	606.	606.	606.	606.	606.	606.	606.	606.	606.	606.	606.	606.
2.	3.	8.	20.	49.	108.	219.	410.	564.	582.	585.	588.	591.	593.	595.	595.	595.	595.	595.	595.	595.	595.	595.	595.	595.	595.	595.	595.	595.	595.
2.	3.	8.	20.	49.	108.	218.	407.	558.	574.	577.	580.	582.	584.	585.	585.	585.	585.	585.	585.	585.	585.	585.	585.	585.	585.	585.	585.	585.	585.
2.	3.	8.	20.	48.	107.	217.	404.	551.	566.	568.	571.	573.	574.	575.	575.	575.	575.	575.	575.	575.	575.	575.	575.	575.	575.	575.	575.	575.	575.
2.	3.	8.	20.	48.	107.	216.	401.	543.	557.	560.	562.	563.	565.	565.	566.	566.	566.	566.	566.	566.	566.	566.	566.	566.	566.	566.	566.	566.	566.
2.	3.	8.	20.	48.	106.	215.	397.	535.	549.	551.	553.	554.	555.	556.	556.	556.	556.	556.	556.	556.	556.	556.	556.	556.	556.	556.	556.	556.	556.
2.	3.	8.	20.	48.	106.	213.	393.	527.	540.	542.	544.	545.	546.	546.	547.	547.	547.	547.	547.	547.	547.	547.	547.	547.	547.	547.	547.	547.	547.
2.	3.	8.	20.	48.	105.	211.	388.	519.	531.	533.	535.	536.	537.	537.	537.	537.	537.	537.	537.	537.	537.	537.	537.	537.	537.	537.	537.	537.	537.
2.	3.	8.	20.	47.	104.	210.	384.	511.	522.	524.	526.	527.	528.	528.	528.	528.	528.	528.	528.	528.	528.	528.	528.	528.	528.	528.	528.	528.	528.
2.	3.	7.	19.	47.	103.	207.	379.	503.	514.	516.	517.	518.	519.	519.	520.	520.	520.	520.	520.	520.	520.	520.	520.	520.	520.	520.	520.	520.	520.
2.	3.	7.	19.	46.	102.	205.	374.	495.	506.	507.	508.	510.	510.	511.	511.	511.	511.	511.	511.	511.	511.	511.	511.	511.	511.	511.	511.	511.	511.
2.	3.	7.	19.	46.	101.	203.	369.	487.	497.	499.	500.	501.	502.	502.	503.	503.	503.	503.	503.	503.	503.	503.	503.	503.	503.	503.	503.	503.	503.
2.	3.	7.	19.	45.	98.	196.	355.	466.	475.	477.	478.	479.	480.	480.	480.	480.	480.	480.	480.	480.	480.	480.	480.	480.	480.	480.	480.	480.	480.
1.	2.	6.	16.	39.	84.	165.	291.	374.	381.	382.	383.	384.	384.	385.	385.	385.	385.	385.	385.	385.	385.	385.	385.	385.	385.	385.	385.	385.	385.
1.	2.	5.	14.	33.	70.	135.	232.	294.	299.	300.	301.	301.	301.	302.	302.	302.	302.	302.	302.	302.	302.	302.	302.	302.	302.	302.	302.	302.	302.
1.	2.	4.	11.	27.	57.	108.	181.	226.	230.	231.	231.	231.	232.	232.	232.	232.	232.	232.	232.	232.	232.	232.	232.	232.	232.	232.	232.	232.	232.
1.	1.	4.	9.	21.	45.	84.	138.	171.	174.	174.	174.	175.	175.	175.	175.	175.	175.	175.	175.	175.	175.	175.	175.	175.	175.	175.	175.	175.	175.
1.	1.	3.	7.	17.	34.	63.	103.	127.	129.	129.	129.	129.	129.	129.	129.	129.	129.	129.	129.	129.	129.	129.	129.	129.	129.	129.	129.	129.	129.
1.	1.	2.	5.	12.	26.	47.	75.	92.	93.	94.	94.	94.	94.	94.	94.	94.	94.	94.	94.	94.	94.	94.	94.	94.	94.	94.	94.	94.	94.
0.	1.	2.	4.	9.	19.	34.	54.	66.	67.	67.	67.	67.	67.	67.	67.	67.	67.	67.	67.	67.	67.	67.	67.	67.	67.	67.	67.	67.	67.
0.	0.	1.	3.	7.	13.	24.	38.	46.	47.	47.	47.	47.	47.	47.	47.	47.	47.	47.	47.	47.	47.	47.	47.	47.	47.	47.	47.	47.	47.
0.	0.	1.	2.	5.	9.	17.	26.	31.	32.	32.	32.	32.	32.	32.	32.	32.	32.	32.	32.	32.	32.	32.	32.	32.	32.	32.	32.	32.	32.
0.	0.	1.	1.	3.	6.	11.	18.	21.	22.	22.	22.	22.	22.	22.	22.	22.	22.	22.	22.	22.	22.	22.	22.	22.	22.	22.	22.	22.	22.
0.	0.	0.	1.	2.	4.	8.	12.	14.	14.	14.	14.	14.	14.	14.	14.	14.	14.	14.	14.	14.	14.	14.	14.	14.	14.	14.	14.	14.	14.
0.	0.	0.	1.	1.	3.	5.	8.	9.	10.	10.	10.	10.	10.	10.	10.	10.	10.	10.	10.	10.	10.	10.	10.	10.	10.	10.	10.	10.	10.
0.	0.	0.	0.	1.	2.	4.	5.	6.	7.	7.	7.	7.	7.	7.	7.	7.	7.	7.	7.	7.	7.	7.	7.	7.	7.	7.	7.	7.	7.
0.	0.	0.	0.	1.	2.	3.	4.	5.	5.	5.	5.	5.	5.	5.	5.	5.	5.	5.	5.	5.	5.	5.	5.	5.	5.	5.	5.	5.	5.
0.	0.	0.	0.	1.	1.	2.	4.	4.	4.	4.	4.	4.	4.	4.	4.	4.	4.	4.	4.	4.	4.	4.	4.	4.	4.	4.	4.	4.	4.

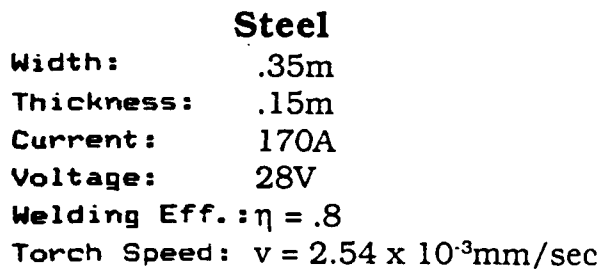
.0225m

.09m

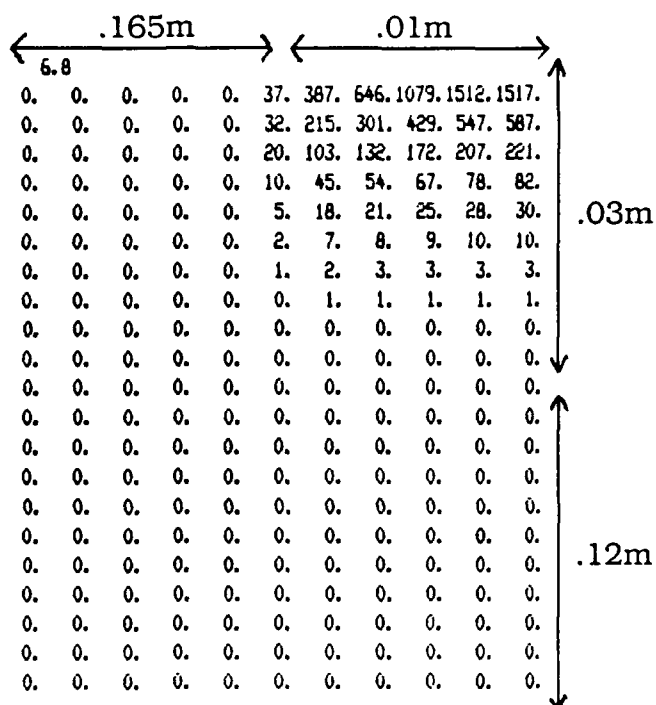
AL

Thickness: .1125m
Width: .2625m
Current: 170A
Voltage: 28V
Welding Eff.: $\eta = .8$
Torch Speed: $v = 2.54 \text{ mm/sec}$

31 x 31



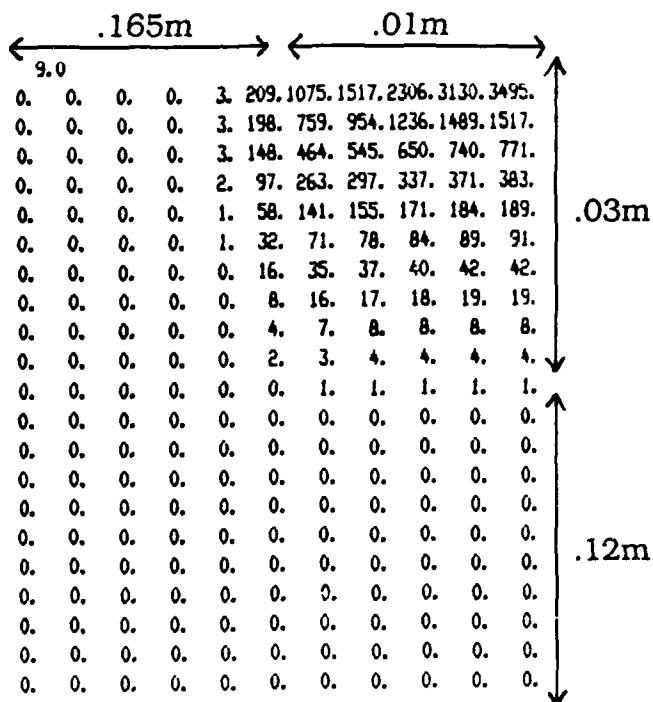
75



Steel

Width: .35m
Thickness: .15m
Current: 170A
Voltage: 28V
Welding Eff.: $\eta = .8$
Torch Speed: $v = 2.54 \text{ mm/sec}$

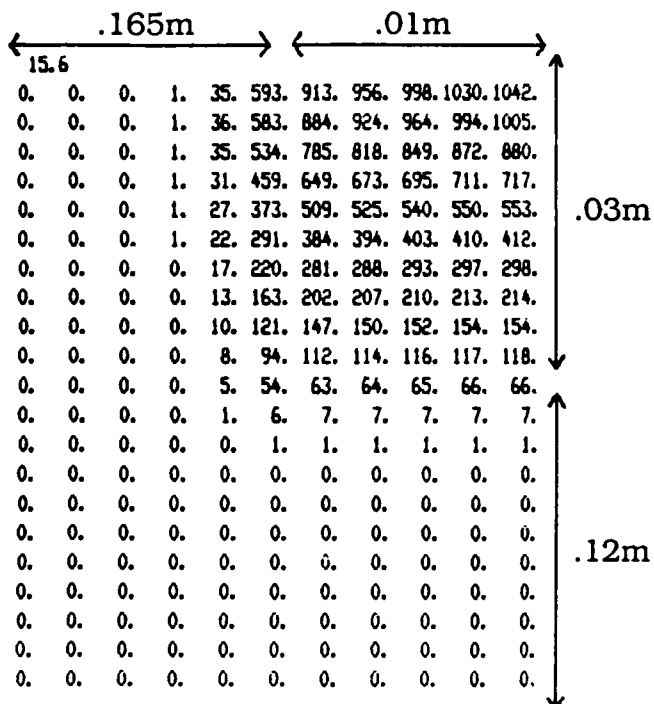
21 x 21



Steel

Width: .35m
 Thickness: .15m
 Current: 170A
 Voltage: 28V
 Welding Eff.: $\eta = .8$
 Torch Speed: $v = 2.54 \text{ mm/sec}$

21 x 21



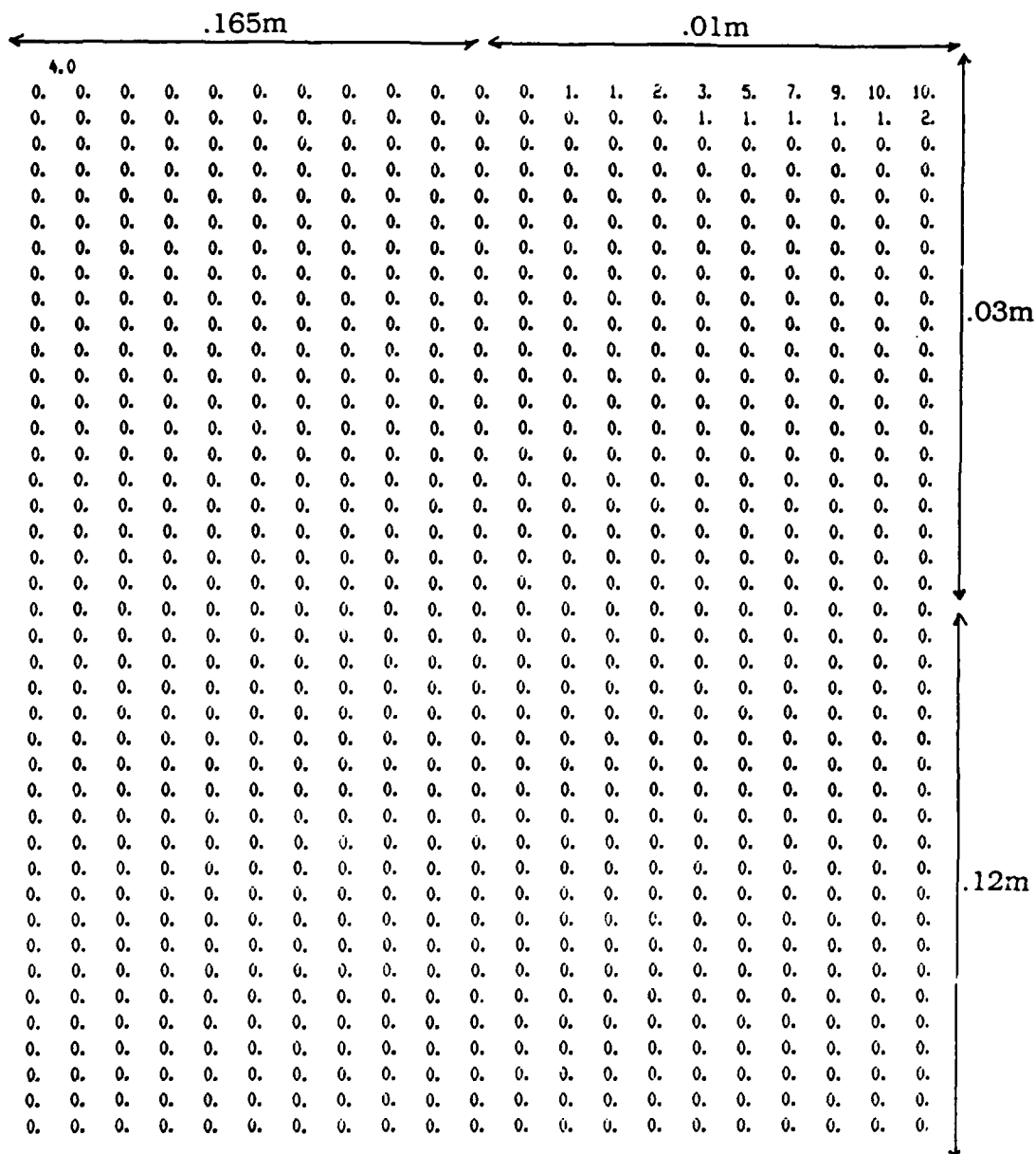
Steel

Width: .35m
 Thickness: .15m
 Current: 170A
 Voltage: 28V
 Welding Eff.: $\eta = .8$
 Torch Speed: $v = 2.54 \text{ mm/sec}$

21 x 21



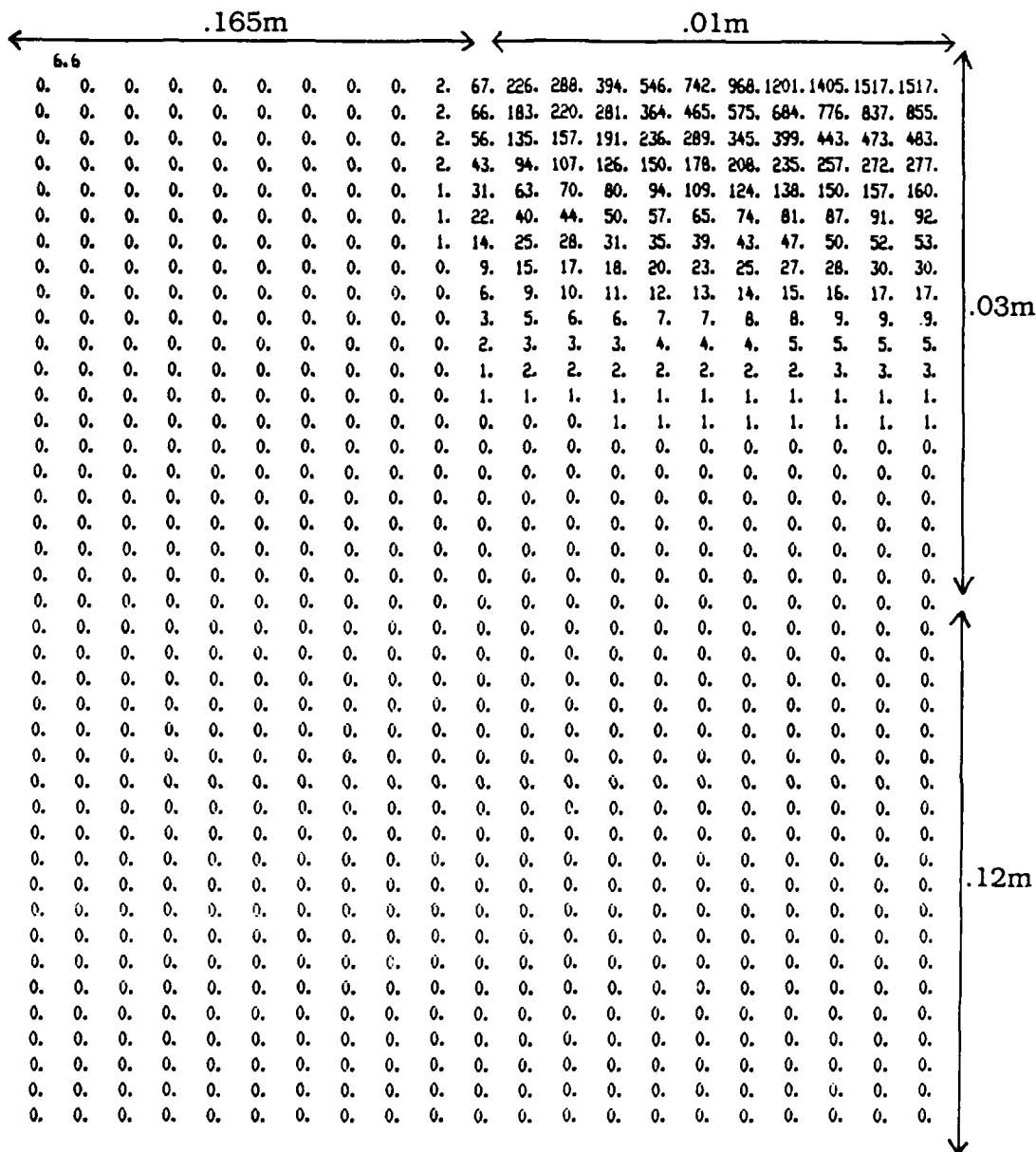
31 x 31



Steel

Thickness / Current: .15m 170A
 Width / Welding Eff.: .35m $\eta = .8$
 Voltage / Torch Speed: 28V $v = 2.54 \text{ mm/sec}$

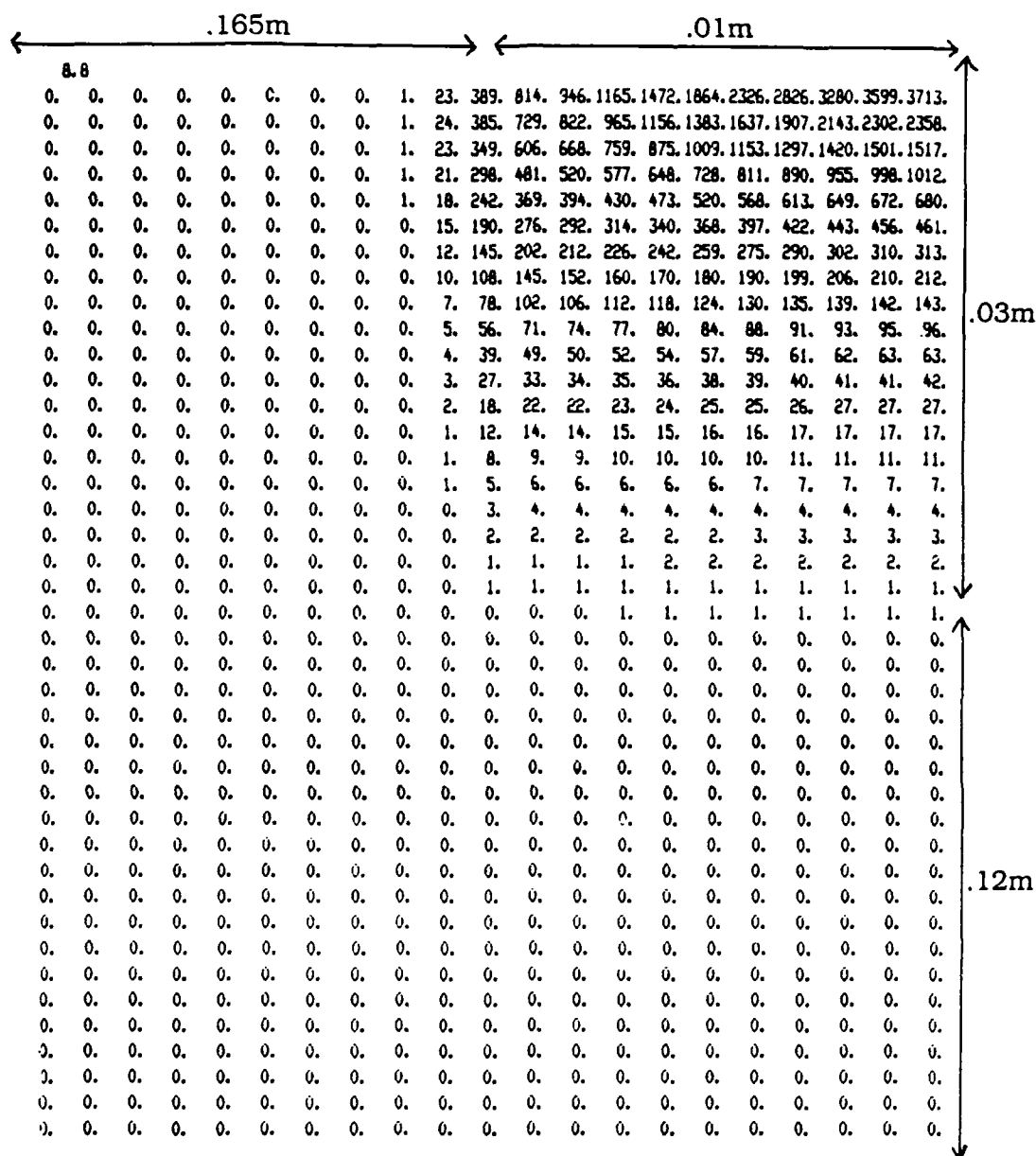
41 x 41



Steel

Thickness / Current: .15m 170A
Width / Welding Eff.: .35m $\eta = .8$
Voltage / Torch Speed: 28V $v = 2.54 \text{ mm/sec}$

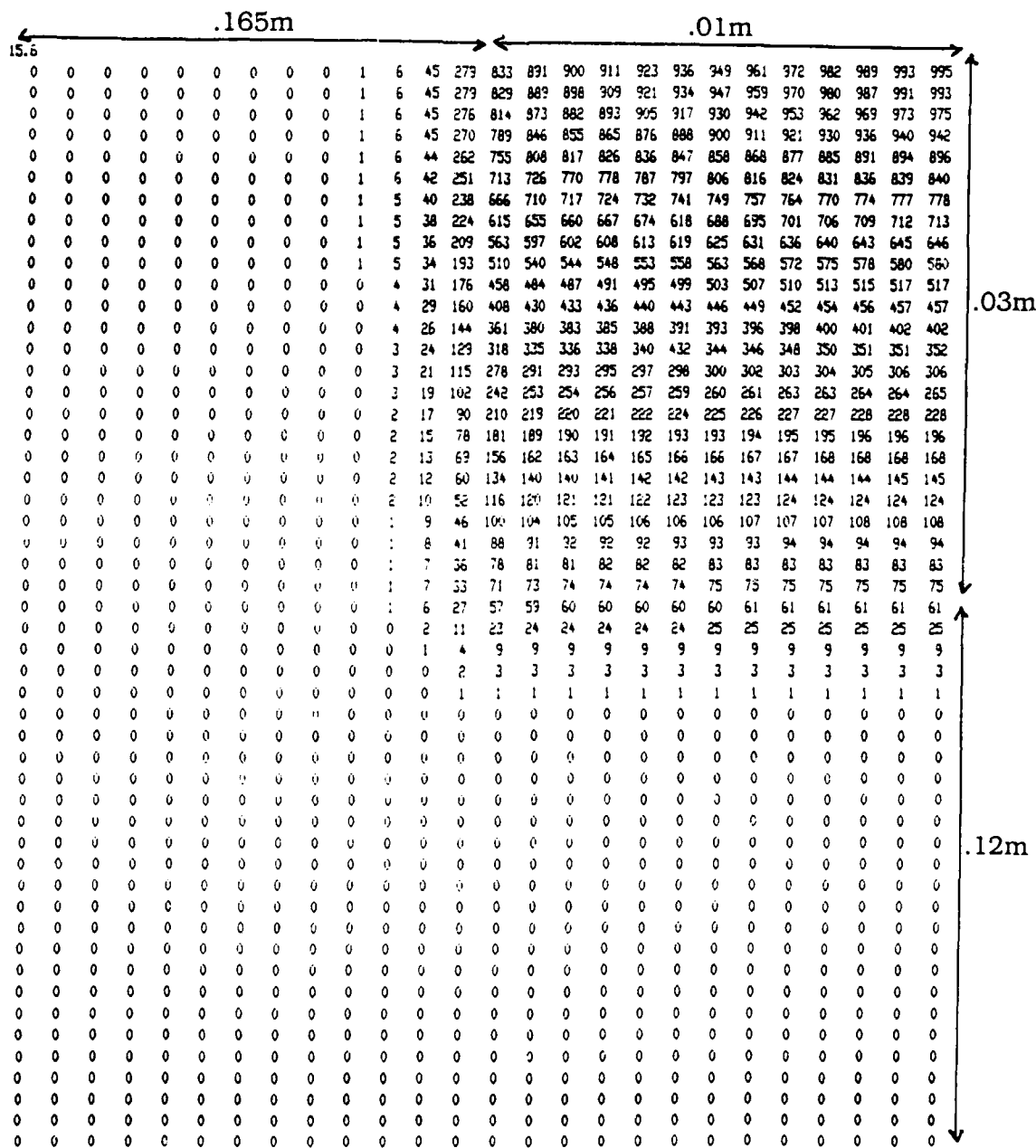
41 x 41



Steel

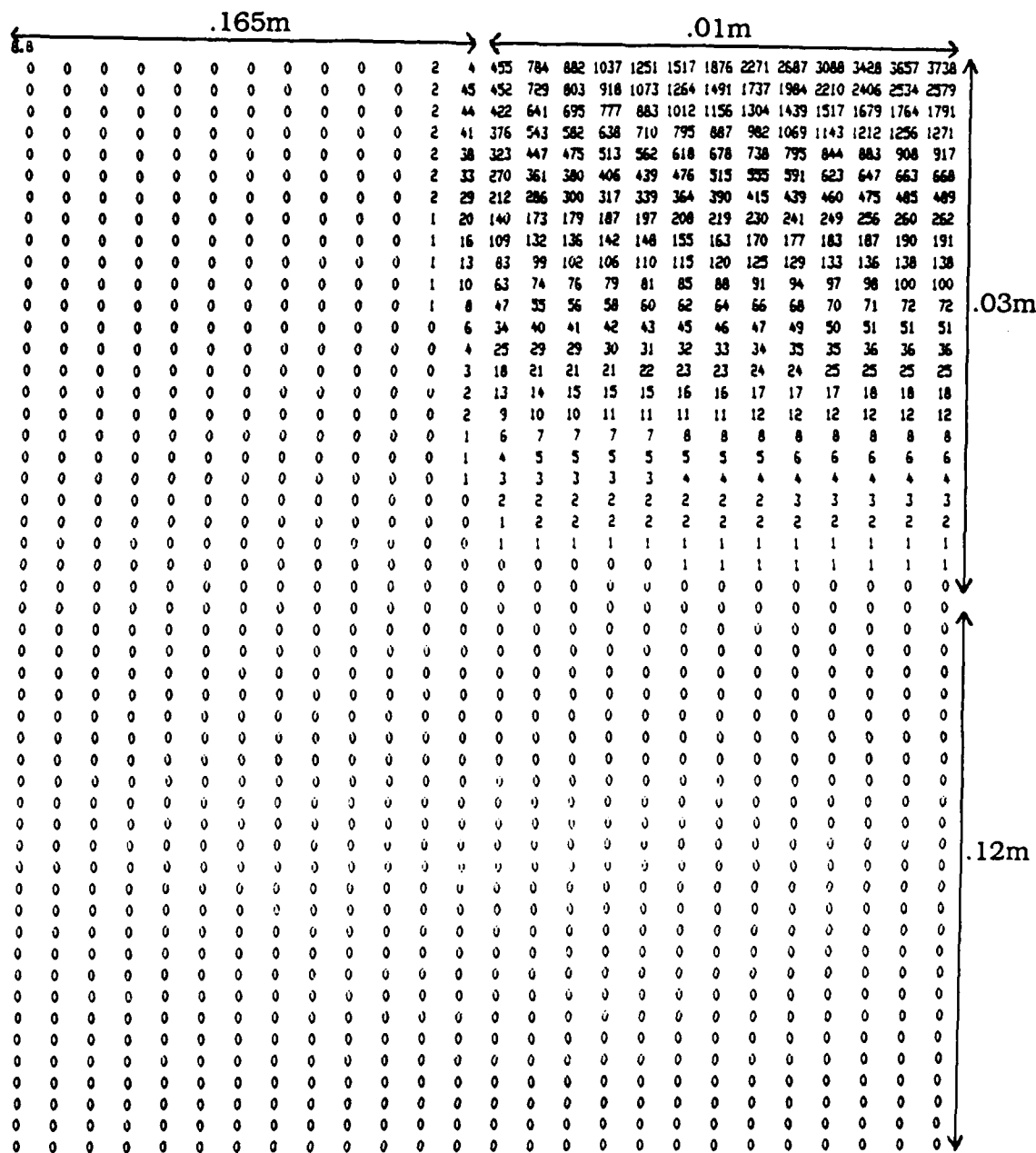
Thickness / Current: .15m 170A
Width / Welding Eff.: .35m $\eta = .8$
Voltage / Torch Speed: 28V $v = 2.54 \text{ mm/sec}$

41 x 41



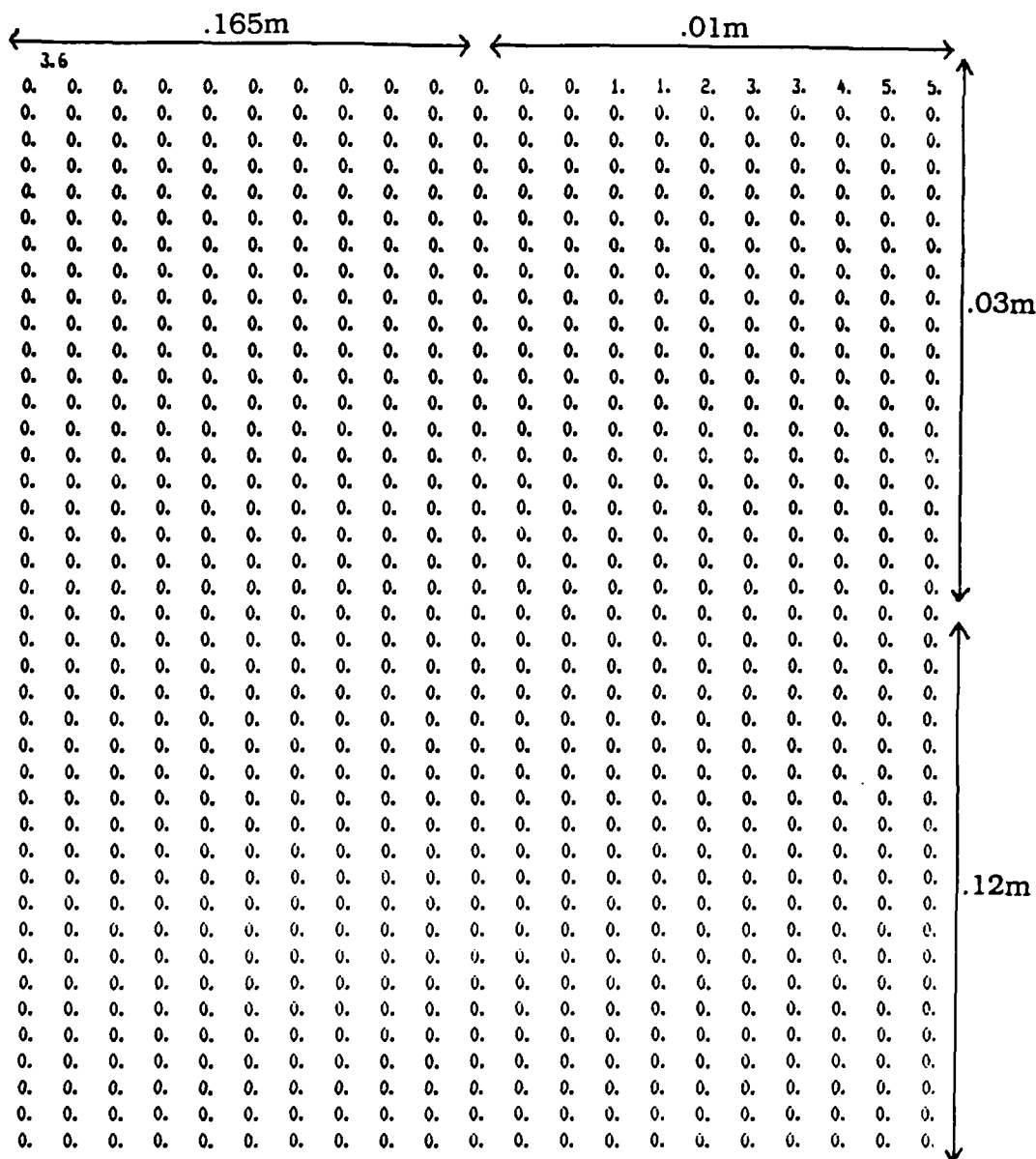
Steel

Thickness / Current: .15m 170A
 Width / Voltage: .35m 28V
 Welding Eff. / Torch Speed: $\eta = .8$ $v = 2.54 \text{ mm/sec}$
 51 x 51



Steel

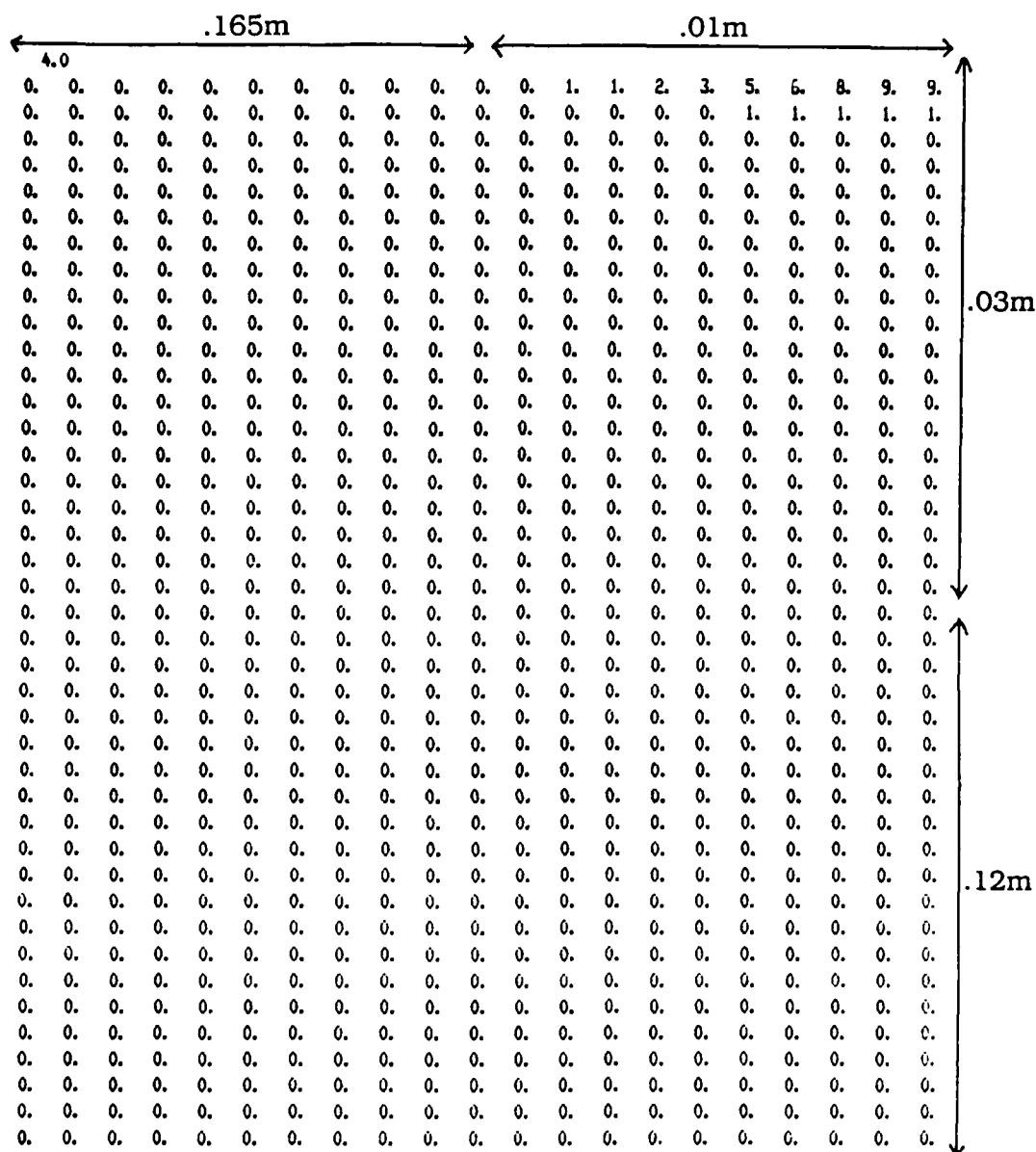
Thickness / Voltage: .15m 28V
 Width / Welding Eff.: .35m $\eta = .8$
 Current / Torch Speed: 170A $v = 2.54 \text{ mm/sec}$
 51 x 51



Steel

Width	/ Voltage:	.35m	28V
Thickness	/ Welding Eff.:	.15m	$\eta = .8$
Current	/ Torch Speed:	170A	$v = 2.794 \text{ mm/sec}$

41 x 41



Steel

Width / Voltage: .35m 28V
 Thickness / Welding Eff.: .15m $\eta = .8$
 Current / Torch Speed: 153A $v = 2.54 \text{ mm/sec}$

41 x 41

LIST OF REFERENCES

1. Masubuchi, K., *Analysis of Welded Structures*, pp. 60-87, Pergamon Press, 1980.
2. Giedt, W. H., "Welding—An Interdisciplinary Science and Technology," *Interdisciplinary Issues in Materials Processing and Manufacturing*, vol. 2, pp. 403-418, The American Society of Mechanical Engineers, 1987.
3. Friedman, E., "Thermomechanical Analysis of the Welding Process Using the Finite Element Method," *Transactions of the ASME, Journal of Pressure Vessel Technology*, vol. 97, Series J, no. 3, pp. 206-213, 1975.
4. Goldak, J., Chakravarti, A., and Bibby, M., "A New Finite Element Model for Welding Heat Sources," *Metallurgical Transactions B*, vol. 15B, pp. 299-305, June 1984.
5. Kou, S., and Le, Y., "Heat Flow During the Autogenous GTA Welding of Pipes," *Metallurgical Transactions A*, vol. 15A, pp. 1165-1171, June 1984.
6. Oreper, G. M., and Szekely, J., "A Comprehensive Representation of Transient Weldpool Development in Spot Welding Operations," *Metallurgical Transactions A*, vol. 18A, pp. 1325-1332, July 1987.
7. Khan, M. A., Madsen, N. H., Goodling, J. S., and Chin, B. A., "Infrared Thermography as a Control for the Welding Process," *Optical Engineering*, vol. 25, no. 6, pp. 779-805, June 1986.
8. Pavelic, R., Tanbakuchi, R., Uyehara, O. A., and Myers, P. S., *Welding Journal Research Supplement*, vol. 48, pp. 295s-305s, 1969.
9. Lunardini, V. J., *Heat Transfer in Cold Climates*, pp. 353-470, Van Nostrand Reinhold Company, 1981.
10. Patankar, S. V., *Numerical Heat Transfer and Fluid Flow*, p. 54, McGraw-Hill, 1980.
11. Touloukian, Y. S., *Thermophysical Properties of Matter*, vol. I, pp. 925 and 1183; vol. IV, pp. 4 and 687, IFI/Plenum, 1979.

12. Incropera, F. P., and DeWitt, D. P., *Introduction to Heat Transfer*, pp. 213-217, John Wiley & Sons, 1985.

INITIAL DISTRIBUTION LIST

	<u>No. Copies</u>
1. Defense Technical Information Center Cameron Station Alexandria, VA 22304-6145	2
2. Library, Code 0142 Naval Postgraduate School Monterey, CA 93943-5002	2
3. Assistant Professor Yogendra Joshi Department of Mechanical Engineering Naval Postgraduate School Monterey, CA 93943-5000	1
4. Professor Anthony J. Healey Department of Mechanical Engineering Naval Postgraduate School Monterey, CA 93943-5000	1
5. Richard A. Morris David Taylor Research Center Code 2815 Annapolis, MD 21402	1
6. LCDR Lambert R. Walker III, U.S. Navy RFD #3 Bennett Road Durham, NH 03824	1